Reviews in Mineralogy & Geochemistry
Vol. 77 pp. 73-121, 2013
Copyright © Mineralogical Society of America

Thermodynamics of Carbonates

A.V. Radha and A. Navrotsky*

Peter A. Rock Thermochemistry Laboratory and
NEAT ORU (Nanomaterials in the Environment, Agriculture,
and Technology Organized Research Unit)
University of California Davis
Davis, California 95616, U.S.A.

ravenkat@ucdavis.edu
*corresponding author: *anavrotsky@ucdavis.edu*

INTRODUCTION

The goal of geologic CO_2 sequestration is not just to pump large volumes of supercritical carbon dioxide into underground repositories but to keep it there for hundreds to thousands of years, preferably in chemically bound form. The permanence of CO_2 storage in geological repositories is important since large leakage rates would diminish the CO_2 abatement achieved with carbon capture and sequestration (CCS). Effective permanent geologic CO_2 storage depends ultimately on the interactions of the supercritical CO_2 with the minerals and fluids present in the host underground repositories and their caprock sealing (Xu et al. 2005; Kharaka et al. 2006, 2010; Benson and Cole 2008). Migration of supercritical CO_2 within these geological repositories is controlled by confinement/trapping of CO_2 in the porous structure as well as solubility of CO_2 in the fluids (brine and hydrocarbons) already present in the storage formation (Cole et al. 2010; Doughty 2010). In deep saline aquifers, the dissolution of CO_2 in water generates carbonic acid, which in turn reacts with minerals such as clay, mica and feldspar and carbonates present in the reservoir rocks to generate cations and carbonate/bicarbonate ions (Kaszuba et al. 2003, 2005; Kharaka et al. 2006; Ketzer et al. 2009; Cole et al. 2010; Doughty 2010). Finally, precipitation of metal carbonate occurs either by direct or indirect reaction of the CO_2 with other minerals and organic matter present in the reservoirs (Garcia et al. 2012; Kharaka et al. 2010; Shao et al. 2010, Xu et al. 2004, 2005).

It is essential to understand and predict the chemical reactions and stability of mineral phases formed under sequestration conditions as these could affect the migration of CO_2 and the seal integrity of the geologic reservoir (Kharaka et al. 2006, 2010; Benson and Cole 2008). Carbonation reactions of cations that exist in formation fluids and the transformation of minerals present in the host rocks into metal carbonates would produce the most permanent and desirable form of subsurface CO_2 storage (Xu et al. 2004, 2005; Ketzer et al. 2009). Carbonation and dissolution/precipitation of silicates changes the solid volume in the caprocks, which potentially can lead to either sealing of existing cracks and micropores or the creation of new porosity, depending on where old minerals dissolve and new ones precipitate and on the volume change of the reactions (Matter and Kelemen 2009). Basalt and peridotite rich in Ca, Mg, Mn and Fe silicates, olivine, serpentine, pyroxene and plagioclase, are considered to have the highest potential to react with dissolved CO_2 in water to precipitate solid carbonates (Ferrini et al. 2009; Matter and Kelemen 2009). However, several geological sites under consideration for sequestration are in sedimentary basins and consist of sandstone, siltstone, and shale made up of minerals such as quartz, clay, dolomite, gypsum, anhydrite, and halite. Though simple carbonates, $CaCO_3$, $MgCO_3$, $FeCO_3$, $MnCO_3$ and their solid solutions are

1529-6466/13/0077-0003$05.00 http://dx.doi.org/10.2138/rmg.2013.77.3

commonly considered to be the main carbonation products, a number of other carbonates and mineral phases containing both carbonate and silicate in their structures have been reported and their formation along with metal carbonates must be considered to better characterize long term geologic CO_2 sequestration.

Carbonate mineralization is a slow process since it involves complex rock-H_2O/fluid-CO_2 interactions and the kinetic and thermodynamic aspects of these processes are not well understood. The knowledge of both these aspects for carbonate formation is critical in assessing the feasibility and safety of sequestration. This review focuses on the thermodynamic aspects, stressing the energetics of the progression from aqueous solution to possible prenucleation clusters, to amorphous and nanocrystalline carbonate precipitates, and finally to well-crystallized carbonate phases. In addition to the common carbonate phases in the system $CaCO_3$-$MgCO_3$-$FeCO_3$ and $MnCO_3$, some more exotic carbonate and carbonate-silicate phases are also reviewed. Some issues of carbonate stability under a range of conditions broader than those encountered for sequestration are also addressed because they shed light on structure, bonding, and energetics.

SEQUENCES OF CARBONATE CRYSTALLIZATION

The physical principles governing various phase formation are complex and depend on crystal growth ($\Delta G_{\text{Nucleation}} + \Delta G_{\text{Growth}}$) and subsequent phase transformation ($\Delta G_{\text{Phase-trans}}$). As discussed in detail in other chapters in this volume, the thermodynamics, mechanisms, and kinetics of precipitation of carbonates from aqueous solution, especially at the relatively high temperatures and pressures encountered in the possible CO_2 sequestration environment, are still poorly known. Crystal formation by nucleation and growth is a free energy driven phenomenon and reflects solution supersaturation. The initial solution with high free energy reaches the lower equilibrium free energy state by final solid phase formation. Saturation is reached when concentrations (activities) of reactant components in the initial solution equal their equilibrium concentrations (activities) or solubility product (K_{sp}) and the change in free energy (per mole) $\Delta G = -RT\ln K_{sp}$ (R is the gas constant, and T is the absolute temperature). Supersaturation reflects higher concentrations. Saturation and supersaturation can be brought about by changes in reactant concentrations, pH, pCO_2, pressure, or temperature.

According to classical theory, nucleation of a new phase (particle with radius r) is activation energy driven and is associated with interplay between free energy change per molecule of bulk solid ($4\prod r^3\Delta G_{bulk}/3$) and surface ($4\prod r^2\gamma$) formation. The interfacial free energy (γ) is a positive term that destabilizes the nucleus below a critical size. Above critical size, the bulk free energy (proportional to r^3) overcomes the positive free energy (proportional to r^2) due to generation of an interface, and then nucleation and growth can proceed. Consequently, any factors that cause a change in interface energy (γ) influence nucleation. Thus factors such as formation of intermediate metastable phases, surface adsorbed water/ions or presence of foreign substrates are known to alter nucleation, crystal growth, and phase transformation processes.

Under near-ambient conditions, there is increasing evidence that carbonate crystallization occurs not only by classical nucleation and growth (De Yoreo and Vekilov 2003; De Yoreo and Dove 2004; De Yoreo et al. 2007, 2009), but also by various other non-classical mechanisms involving prenucleation clusters, metastable liquid-like precursors, mesocrystals, amorphous and nanophase precursors in the early stages of crystal growth (Gebauer and Coelfen 2011; Navrotsky 2004; Gebauer et al. 2008; Gower 2008; Meldrum and Colfen 2008; Tribello et al. 2009; Raiteri and Gale 2010; Demichelis et al. 2011; Bewernitz et al. 2012). In classical nucleation, the initial random solute clusters formed in a supersaturated solution are thermodynamically unstable and decompose until they reach a critical size, leaving only a very low, dynamic, and transient concentration of such species in solution (see Fig. 1).

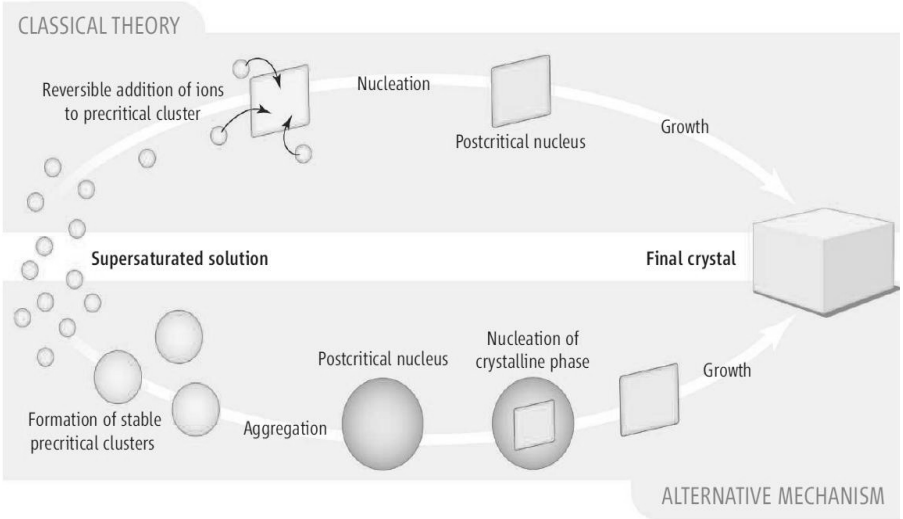

Figure 1. Schematic of carbonate nucleation by (a) classical nucleation theory by addition of ions to a single cluster (top) and (b) alternative mechanism by aggregation of stable, amorphous, precritical clusters (bottom). Reprinted with permission from Meldrum and Sear (2008). Copyright 2008 by the American Association for the Advancement of Science.

In contrast to this classical picture, prior to the carbonate phase nucleation, aqueous solutions often contain "prenucleation clusters", groupings of cations, carbonate groups and water that are intermediate in size between molecules and nanophase precipitates. These clusters, that may or may not resemble the final phase, could act as precursors for the precipitation of nanophase carbonates (see Fig. 1). They are often initially heavily hydrated and amorphous to X-ray diffraction, as discussed below. They may be a thermodynamic intermediate on the road to solid phases, intermediate in free energy between dissolved ions and nanoparticles. Classical and nonclassical nucleation are discussed in detail by De Yoreo et al. (2013, this volume).

Thermodynamics of prenucleation clusters

Prenucleation clusters were initially detected by careful solubility studies that suggested a lowering of thermodynamic activity of ions in solution, leaving not all Ca^{2+} and CO_3^{2-} "free" to precipitate $CaCO_3$ (Gebauer et al. 2008). This implies that bound states of calcium and carbonate ions in clusters may exist in solution and involve a significant fraction of the concentration of these ions (see Fig. 2). These initial observations have been followed by analytical ultracentrifugation (AUC), spectroscopic and cryo-TEM studies that provided stronger evidence for the existence of clusters of about 2 nm in diameter that can grow by colliding and coalescing (Gebauer et al. 2008; Pouget et al. 2009; Gebauer and Coelfen 2011). The cluster formation reaction can be represented as:

$$zCa^{2+} + zCO_3^{\ 2-} + nH_2O = [CaCO_3]_z \cdot nH_2O$$

Thermodynamic equilibrium for this reaction was established by showing the reversibility of the system with changes in pH and calcium concentration (Gebauer et al. 2008). Unfortunately, unknown cluster structure, size and activity made it impossible to directly determine the thermodynamic equilibrium constant for this reaction. Therefore, in a different approach, the cluster equilibrium was characterized using an ion-binding speciation model with multiple equal and independent equilibrium constants ($K' = K_1 = K_2 = K_3 = \ldots$) as depicted schematically in Figure 3 (Gebauer et al. 2008). The binding strength increases with increased calcium ion bind-

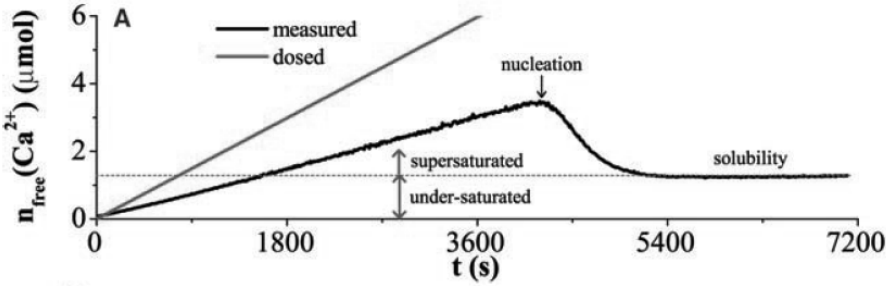

Figure 2. Free calcium ions measured by the calcium ion selective electrode (thick black line) in comparison with the dosed amount of calcium ions (dark grey line) at pH 9.5. The difference between these two gives the bound calcium ions. Reproduced with permission from Gebauer et al. (2008). Copyright 2008 by the American Association for the Advancement of Science.

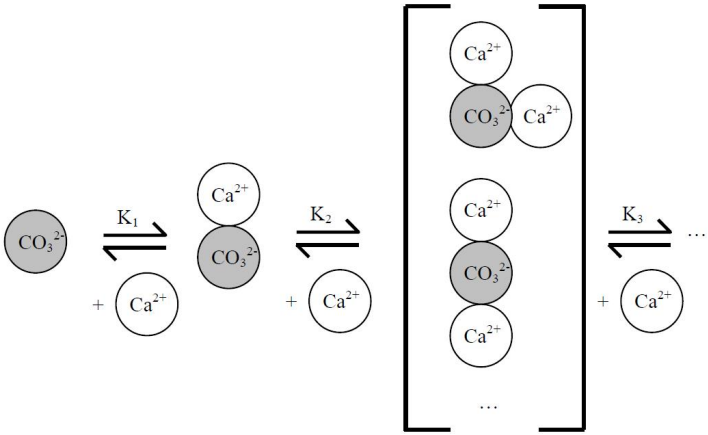

Figure 3. A schematic of multiple-binding equilibrium model depicting a carbonate centre-ion and binding calcium ions. The bracket shows various three dimensional possible bonding structures for the equilibrium steps and the steps are independent with equalized equilibrium constants $K = K_1 = K_2 = K_3$… From supporting information of Gebauer et al. (2008) and is reprinted with permission. Copyright 2008 by the American Association for the Advancement of Science.

ing with carbonate in multiple equal steps and finally attains the macroscopic binding strength (K') similar to ion pair formation in the clusters. Hence one can use the macroscopic binding constant to arrive at the standard free energy of ion pair formation in clusters ($-RT\ln K' = \Delta G_{ion-pair}$). The average amount of bound calcium and carbonate ions could be quantified indirectly using a calcium ion sensitive electrode and constant pH titration for carbonate ions (Gebauer et al. 2008). The difference between measured free calcium ion concentration and the dosed amount corresponds to the amount of bound calcium ions in the clusters. The derived equilibrium constants ($K >> 1$, i.e., $\Delta G < 0$) suggest that the clusters are thermodynamically stable with respect to both free ions as well as ion pairs and correspond to a global Gibbs free energy minimum in the solution phase. The average free energy over several equilibria for ion pair formation in the clusters at pH 8.5 to 9.8 range from −17.3 to −18.5 kJ/mol. The clusters formed at lower pH are found to be thermodynamically more stable than ones formed in higher pH solution. Addition of more calcium ions makes the solution state metastable with respect to a solid phase and aggregation of these clusters leads to the nucleation of amorphous nanoparticles in solution and eventually to the calcite phase through various metastable amorphous and crystalline phases.

Figure 4 shows a schematic free energy profile for amorphous calcium carbonate from ion pairs in solution by the nonclassical mechanism and its evolution to the crystalline phase (Gebauer et al. 2008; Meldrum and Colfen 2008; Pouget et al. 2009; Gebauer and Coelfen 2011).

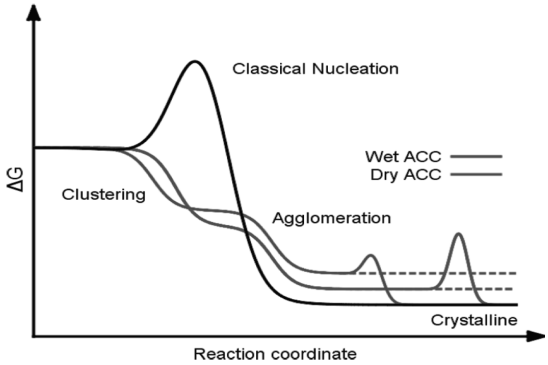

Figure 4. A schematic of free energy profile for calcium carbonate from ion pairs in solution by classical and non-classical methods. Used with permission from Raiteri and Gale (2010). Copyright 2010 by the American Chemical Society.

Prenucleation cluster formation has also been observed in pure magnesium as well as in a mixed calcium and magnesium solution in contact with carbonate ions (Verch et al. 2012). The ultracentrifugation experiments suggest the existence of more than one type of cluster species in pure $MgCO_3$ solutions. In mixed Ca/Mg solutions, the formation of mixed cation pre-nucleation clusters was found to be favored over pure $CaCO_3$ and $MgCO_3$ clusters. In addition, in mixed clusters calcium enrichment over magnesium was observed with respect to the solution composition over the entire Ca/Mg composition range. This could explain high magnesium contents observed in biogenic amorphous calcium carbonates (Gebauer and Coelfen 2011; Verch et al. 2012).

Cluster formation in the early stages of carbonate formation was also suggested by several computational studies (Quigley and Rodger 2008; Tribello et al. 2009; Raiteri and Gale 2010; Raiteri et al. 2010). These studies proved to be very useful in overcoming the experimental difficulties in obtaining the thermodynamic data for cluster formation. Molecular dynamics studies on growth of calcium carbonate in water suggested calcium-carbonate ion pairs binding in clusters is exothermic and falls in the range of −10 and −16 kJ/mol (Raiteri and Gale 2010; Raiteri et al. 2010). The free energy profiles from ion pair binding to clusters to amorphous calcium carbonate (ACC) showed no systematic change in binding energy as a function of increasing size (see Fig. 5). This profile shows a very small (nearly zero) activation energy for the cluster growth process in ACC. The two minima at distances of 2.5-4 Å are due to inclusion of ion pairs into the cluster. These minima become deeper at the point where clusters transform into an ACC precipitate. Therefore, the growth of ACC proceeds without any thermodynamic energy barriers as opposed to a large barrier to calcite crystal growth. Though calcite nanocrystals are stable in solution, at high supersaturation, particles of amorphous material form because they grow much faster than the calcite nanocrystals. The two steps of formation of an ion pair and binding of this ion pair to the cluster in the simulation actually represent ion pair formation in clusters. The average free energy changes for these two steps (the midpoint of the energy range, −20 kJ/mol, gives the free energy of formation of an ion pair in a cluster. This value is in good agreement with the experimentally measured value by Gebauer et al. (−18.5 kJ/mol at pH 8.5). These computational studies match with the experimental data and support the experimental observation of stable prenucleation clusters (Gebauer et al. 2008; Gebauer and Coelfen 2011; Verch et al. 2012).

Thermodynamics of metastable liquid precursors

Calcium carbonate nucleation has also been suggested to occur by a liquid-liquid phase separation mechanism with formation of tiny droplets of a calcium carbonate rich solution from the bulk solution (Gower 2008; Bewernitz et al. 2012). This phenomenon, also known

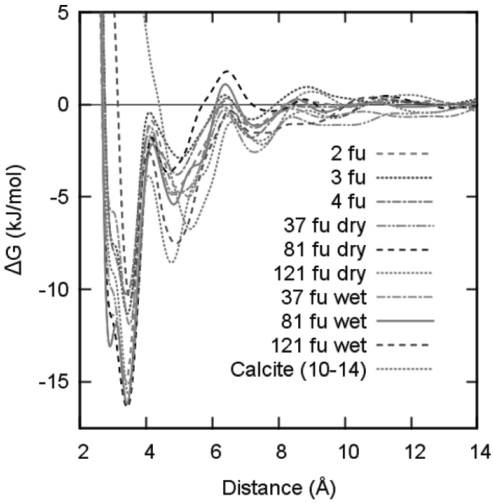

Figure 5. Computed free energy profiles for addition of $CaCO_3$ ion pair to clusters in anhydrous amorphous calcium carbonate and calcite (104) surface. The label of (n + 1) fu indicates the final state of the cluster with (n+1) number of formula units. Used with permission from Raiteri and Gale (2010). Copyright 2010 by the American Chemical Society.

as a polymer induced liquid precursor process (PILP), was first reported by Gower et al. (2008) during calcium carbonate film formation in presence of polyaspartate and was initially thought to be a polymer additive mediated process. Later, evidence of the existence of a liquid drop phase was also demonstrated by acoustic levitation, cryo-TEM and CO_2 outgassing techniques (Faatz et al. 2004; Rieger et al. 2007; Wolf et al. 2011). The thermodynamics of phase separation or PILP formation in the $CaCO_3$ system has been investigated by directly measuring the enthalpy change during punctuated injection of aqueous $CaCl_2$ to a bicarbonate buffer using isothermal titration calorimetry with and without polymer additives (Bewernitz et al. 2012). The enthalpy measurements showed an endothermic process with a discontinuous trend characteristic of a first order phase transition (see Fig. 6). The endothermic enthalpy for liquid droplet formation strongly suggests a major entropic contribution for its stabilization.

In addition, the phase evolution in a similar titration was characterized by a combination of several experimental techniques (light scattering, analytical ultracentrifugation and ^{13}C NMR) (Bewernitz et al. 2012). These studies suggested the emergence of droplets (60 nm size) at the first order transition point, which grew into larger drops of a calcium carbonate rich phase on addition of more Ca^{2+} to the solution. Unlike prenucleation clusters, the liquid condensed phase had a significant amount of calcium bicarbonate ion pairs, which led to an additional energy barrier due to deprotonation of bicarbonate ions during the nucleation of calcium carbonate particles (see Fig. 7). This mechanism thus can lead to ACC formation since crystallization has a large barrier.

Molecular dynamics simulations also showed the formation of stable ionic polymers consisting of linear or branched chains of cations and carbonate/bicarbonate prior to nucleation. These were called dynamically ordered liquid-like oxyanion polymers (DOLLOP) (Demichelis et al. 2011). The chains grew longer on collisions with ions/ion pairs and showed flexibility to distortion similar to a liquid droplet since the free energy cost for changes in radius of gyration is less than ambient thermal energy. The computed free energies for speciation of different ion pairs from this study are listed in Table 1. The transition from DOLLOP to ACC occurs with a significant activation barrier as it involves dehydration of DOLLOP, supporting earlier experimental prediction (Plummer and Busenberg 1982).

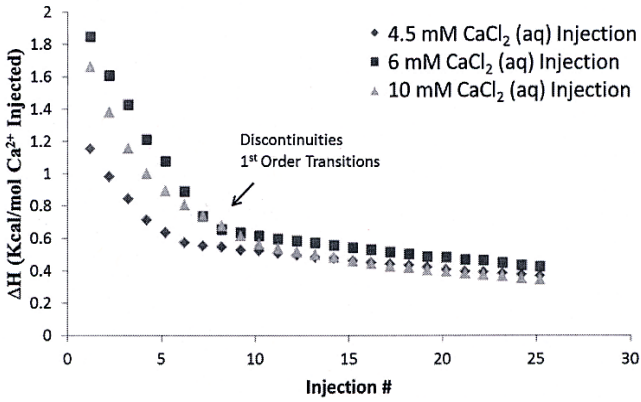

Figure 6. The enthalpy of reaction during the titration of $CaCl_{2(aq)}$ into 20 mM carbonate buffer, pH 8.5. Reprinted from Bewernitz et al. (2012) with permission. Copyright © 2012 Royal Society of Chemistry.

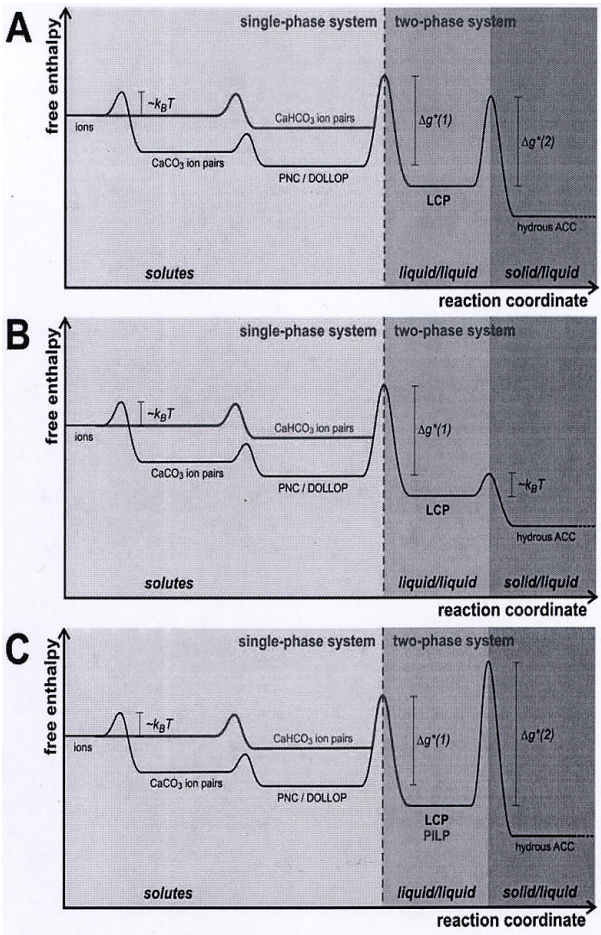

Figure 7. The energetics of calcium carbonate precipitation from supersaturated solution. (A) At neutral pH, nucleation occurs with calcium bicarbonate species with intrinsic kinetic stabilization, $\Delta G^*(2)$. (B) At higher pH, $\Delta G^*(2)$ almost vanishes due to negligible calcium bicarbonate ion pairing and carbonate species dominate the nucleation process with transient liquid condensed phase LCP. (C) In the presence of PAsp polymer, the $\Delta G^*(2)$ barrier increases due to a pronounced role of bicarbonate species in the LCP. Reprinted from Bewernitz et al. (2012) with permission. Copyright © 2012 Royal Society of Chemistry.

Table 1. Free energies from molecular dynamic simulations for three reactions obtained by ion pair speciation model at 0.5, 0.28 and 0.06 M. Reproduced with permission from Demichelis et al. (2011). Copyright © 2011 Nature Publishing Group.

Reaction	Free energies (kJ/mol)		
	pH 9.5	pH 10	Fit to all pHs
$Ca^{2+} + HCO_3^- \rightarrow CaHCO_3^+$	−11.4	−11.4	−11.3
$Ca^{2+} + CO_3^{2-} \rightarrow CaCO_3^0$	−18.6	−20.5	−20.3
$CaCO_3^0 + (CaCO_3^0)_n \rightarrow (CaCO_3^0)_{n+1}$	−22.9	−22.0	−21.7

Mesocrystallization

Mesocrystallization refers to the organization of nanocrystalline particles with various crystallographic registries by different mechanisms as illustrated in Figure 8. Such assemblies form either by oriented attachment of crystalline nano-bricks with surface functionalized polymeric additives or by crystallization of a dense array of amorphous calcium carbonate (ACC) precursor particles. (Colfen and Antonietti 2008; Meldrum and Colfen 2008)

Amorphous carbonates: Energetics of the $CaCO_3$-$MgCO_3$-$FeCO_3$-$MnCO_3$ system

Recent acid solution calorimetric studies have focused on the energetics of amorphous carbonates (amorphous calcium carbonate = ACC, amorphous magnesium carbonate = AMC, ACC-AMC solid solutions, amorphous iron carbonate = AFC and amorphous manganese carbonate = AMNC). Data are summarized in Table 2.

ACC can be precipitated from aqueous solution below room temperature but it is not persistent, crystallizing in hours or less in contact with its mother liquor and within a few days even when separated and dried. ACC is also formed biogenically as a precursor to calcite or aragonite structures in organisms such as molluscs and sea urchins. Calorimetric study (see Fig. 9) shows a complex energy landscape, with ACC progressively dehydrating to more energetically stable amorphous forms, and then crystallizing to nanocrystalline and finally bulk crystalline carbonate (Radha et al. 2010). ACC can be a precursor for vaterite, aragonite, or calcite, lying higher in energy than any of these crystalline forms (Radha et al. 2010). The ACC crystallization energetics reported by various experimental and computational studies are summarized in Table 3.

The ACC–AMC system with $0 \leq x = Mg/(Mg+Ca) \leq 1$ (see Fig. 10) shows a number of interesting energetic trends (Radha et al. 2012). All solid solution compositions are less metastable than a mixture of the end-members, ACC and AMC (enthalpies of formation from calcite and magnesite less positive for solid solutions than for mechanical mixture). There is a definite break in the energetic trends near $x = 0.5$, a composition corresponding to dolomite (see Fig. 10). This break separates two roughly linear distinct segments in enthalpy; a "homogeneous region for $x < 0.5$ and a heterogeneous one for $x > 0.5$, the latter showing two sets of decomposition peaks in DSC curves. Although powder XRD confirms the amorphous nature over the entire composition range, $0 < x < 1$, characterization by TGA/DSC coupled with FTIR suggests heterogeneous (pseudo two phase) behavior for samples with $0.5 < x < 1$ (Radha et al. 2012). All these data support the coexistence of a mixture of AMC with an amorphous material with composition near $x = 0.5$ for Mg-rich bulk compositions with $x > 0.5$. The length scale of this phase separation may be higher than the coherent domain size and short range order interrogated by the X-ray pair distribution functions (PDF) as the PDF data are not conclusive in determining the existence of heterogeneity (Radha et al. 2012).

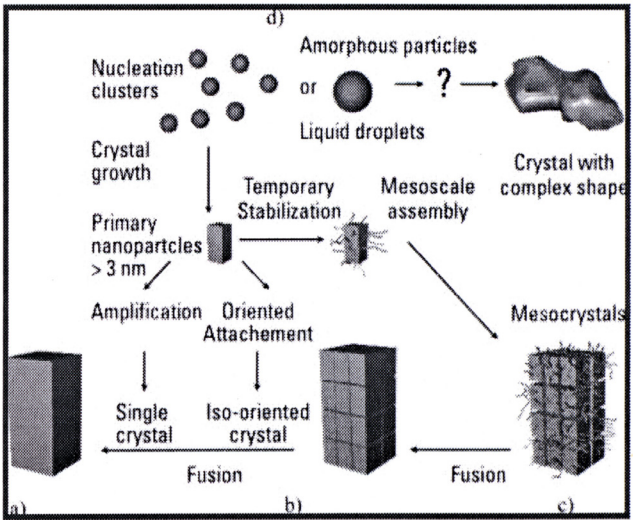

Figure 8. Schematic representation of (a) classical crystal nucleation and growth of a single crystal via primary nanoparticle, (b) single crystal formation from iso-oriented crystal due to oriented attachment of primary nanoparticles (c) mesocrystal formation either from a polymer or additive covered primary nanoparticles or directly from pure nanoparticle and (d) formation of amorphous particles and its transformation to complicated morphologies. Reprinted with permission from Colfen and Antonietti (2008). Copyright 2008 John Wiley & Sons.

Table 2. Calorimetric data for amorphous carbonate phases and corresponding water content per MCO_3. Reproduced with permission of Elsevier Science from Sel et al. (2012). Copyright © 2012 Elsevier Science.

Amorphous $MCO_3 \cdot nH_2O$	Water from TGA (n) (mol)	Enthalpy of Crystallization (ΔH_{crys}) (kJ/mol)	Ionic/crystal radius M^{2+} (nm)	Refs.
$MnCO_3 \cdot nH_2O$ (AMNC)	1.2 ± 0.04	−32.44± 0.71	0.083 (0.097)	[1]
$CaCO_3 \cdot nH_2O$ (ACC)	1.13 - 1.58	−17 ± 1 to −24 ± 1	0.1 (0.114)	[2]
$MgCO_3 \cdot nH_2O$ (AMC)	1.28	−35.8 ± 1.2	0.072 (0.086)	[3]
$FeCO_3 \cdot nH_2O$ (AFC)	1.75	−37.8 ± 9.8	0.078 (0.092)	[4]

The values in () is crystal radius.
References: [1] Radha and Navrotsky (in prep); [2] Radha et al. (2010); [3] Radha et al. (2012); [4] Sel et al. (2012)

The enthalpies of crystallization in the homogeneous region vary roughly linearly with x and range from −10.6 ± 0.8 to −16.9 ± 0.6 kJ/mol. Interestingly, the crystallization enthalpy measured for the biogenic spicule sample containing about 5 mol% $MgCO_3$ extracted from California purple sea urchin larval spicules (−13.3 ± 0.5 kJ/mol) falls in this region (Radha et al. 2010). The overlaid histogram in Figure 10 shows the number of reported biominerals containing different amounts of Mg (Addadi et al. 2003). It can be seen that the Mg content in biominerals varies between $x = 0$ and $x = 0.3$ coincides with the low metastability portion of this region ($0.02 < x < 0.20$) (Beniash et al. 1997; Aizenberg et al. 2002; Addadi et al. 2003). This observation suggests that the marine organisms may select this single-phase low-metastability pathway for calcification by controlling the Mg uptake in the early stages of

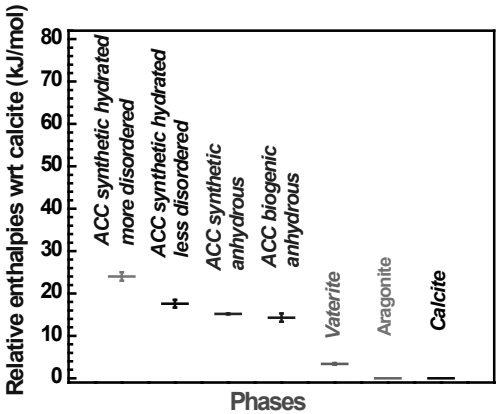

Figure 9. Energetic stabilities of different calcium carbonate phases with respect to calcite. The enthalpy values of vaterite and aragonite are taken from Wolf et al. (2000) and Wolf et al. (1996) respectively. Reprinted from Radha et al. (2010) with permission of the National Academy of Sciences, USA. Copyright © 2010 National Academy of Sciences, USA.

Table 3. Experimental and computational energetic data on various $CaCO_3$ phases with respect to calcite. Modified from Wang and Becker (2012).

ACC	Disordered Vaterite	Ordered Vaterite	Aragonite	Method	Refs.
+26.6	20.7	9.7	–3.0	MD simulations	[1]
+28.5				MD simulations	[1]
			–4.8	MD Force fields	[2]
			12.67	MD Force fields	[2]
		5.0	8.6	DFT (DMol3) plane wave	[1]
	16.39	2.95	0.996	DFT (CASTEP) plane wave	[1]
	17.54	5.72	12.69	DFT (CASTEP) ultrafast pseudopotential	[1]
	19.8	5.8	12.19	DFT (VASP and GGA-PAW)	[1]
			–4.9	DFT (SIESTA) linear scaling	[2]
			+9.3		[2]
+15.0				Thermoanalysis	[3]
+14.3				Anhydrous ACC by calorimetry	[4]
+22.7				More disordered ACC by calorimetry	[4]
+17.2				Less disordered ACC by calorimetry	[4]
+12.3				Thermal analysis	[5]
	6.2		1.2	Dissociation reactions	[6]
	3.4		–0.4	Calorimetric and potentiometric methods	[7]

References: [1] Wang amd Becker (2009, 2012); [2] Raiteri et al. (2010); [3] Wolf and Gunther (2001); [4] Radha et al. (2010); [5] Koga et al. (1998); [6] Plummer and Busenberg (1982); [7] Wolf et al. (1996, 2000)

biomineralization. An earlier study (Wang et al. 2009) suggests that the electrostatic potential around carboxyl groups in proteins regulates Mg uptake, probably by assisting the dehydration of the Mg^{2+} ions, i.e., by assisting the kinetics of Mg^{2+} incorporation. Calorimetric studies suggest that there is an additional thermodynamic driving force to the incorporation of Mg^{2+} into biominerals. It is also interesting that the materials with $x < 0.20$ crystallize more readily than those with higher Mg content. The ability to tune crystallization rates on time scales of hours to days (rather than weeks to months) may be another reason organisms control the Mg content of the amorphous carbonate precursors to be in this range.

The water content appears to influence the enthalpies of crystallization and hence the metastability of samples. The enthalpies of crystallization of more hydrated samples deviate

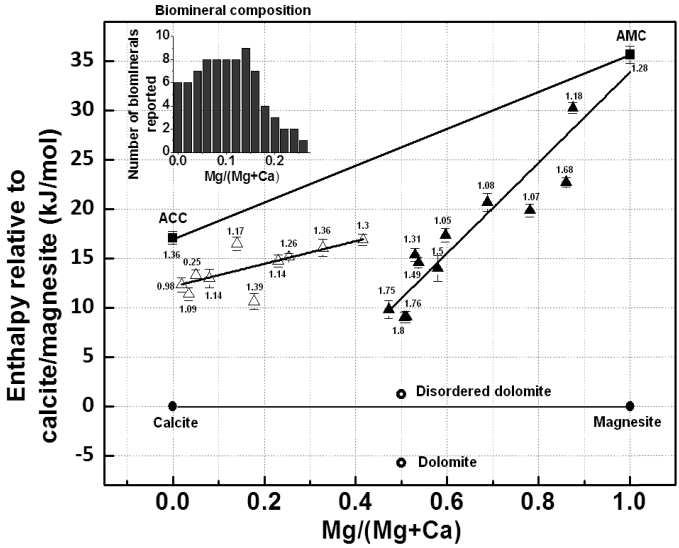

Figure 10. Energetic stabilities of amorphous $Ca_{1-x}Mg_xCO_3 \cdot nH_2O$ ($0 \leq x \leq 1$) phases with respect to calcite and magnesite. Open triangles are for homogeneous single phase region and filled triangles represent potentially heterogeneous two phase region. The inset is the histogram of number of binominals as function of their Mg contents (Addadi et al. 2003). The values of disordered dolomite and dolomite are taken from Navrotsky and Capobianco (1987) and Chai et al. (1995). The number on each symbol is the water content of corresponding amorphous phase. Reprinted from Radha et al. (2012) with permission from Elsevier Science. Copyright © 2012 Elsevier Science.

from the linear trend to less exothermic enthalpies of crystallization in both regions, which indicates lower energetic metastability of more hydrated amorphous materials. The most hydrated samples occur at x = 0.47 to 0.51 and have the least exothermic enthalpies of crystallization in the whole system (see Fig. 10). The Mg/Ca ratio in this range is similar to that in dolomite. This suggests that this region, having lesser metastability, could be an amorphous precursor to dolomite formation.

The more exothermic crystallization enthalpy of AMC compared to ACC suggests that AMC is more metastable than ACC. Nevertheless AMC is much more persistent, surviving for a year or more under ambient conditions without crystallizing (Radha et al. 2012). This may be a kinetic effect related to the difficulty of dehydrating the first coordination sphere of the Mg^{2+} ion. The low temperature decomposition of AMC (432 °C) without any sign of crystallization indicates that AMC is thermally less stable than ACC (771 °C). Magnesite, the stable crystalline form of $MgCO_3$, appears to form only under high temperature synthesis conditions either by hydrothermal methods or by reaction of MgO with CO_2. Hence AMC does not appear to be a precursor phase to magnesite and the possible significance of AMC formation in carbonate mineralization under various conditions may require more detailed investigation.

The energetics of the amorphous iron carbonate (AFC) precursor formed during siderite precipitation has been measured by high-temperature oxide-melt solution calorimetry (Sel et al. 2012). The synthesis, isolation and characterization of AFC require maintenance of anaerobic condition (in nitrogen glove box) to prevent Fe^{2+} oxidation and probably for this reason there is not much report of synthetic AFC in the literature. Thermal decomposition of AFC on heating is complex and the oxide phases formed at the end of decomposition are different in inert and oxidizing conditions. In an inert Ar atmosphere, the DSC profile of AFC shows an endothermic

peak near 120 °C due to dehydration and multiple thermal events at 160-325 °C due to simultaneous crystallization (exothermic) and decomposition (endothermic) of $FeCO_3$ to FeO and CO_2. At higher temperature, FeO further reacts with CO_2 (exothermic) to form Fe_3O_4 or Fe_2O_3 and CO gas. Thermal decomposition of AFC in air or oxygen leads to formation of hematite (Fe_2O_3) (for more details, see Sel et al. 2012).

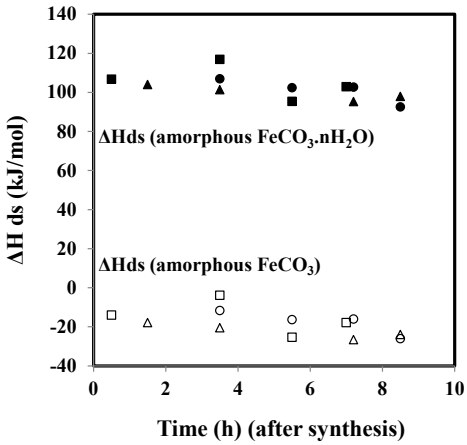

Figure 11. The ethalpies of drop solution ΔH_{ds} data of amorphous iron (II) carbonate (AFC) as a function of time after their synthesis for three different samples. ΔH_{ds} (amorphous $FeCO_3$) is for anhydrous sample corrected for water determined from the TGA/DSC as physically absorbed water. Reproduced with permission of Elsevier Science from Sel et al. (2012). Copyright © 2012 Elsevier Science.

Calorimetric measurements have been done on several freshly prepared samples of AFC to minimize the effects of oxidation (Fe^{2+} to Fe^{3+}), amorphous phase short range structure evolution, and crystallization to siderite. The scatter in the calorimetric data measured within 8-9 h after the synthesis (see Fig. 11) is reasonable considering the sample handling challenges of these highly air sensitive samples. The exothermic crystallization enthalpy (−37.8 ± 9.8 kJ/mol) of AFC suggests that amorphous $FeCO_3$ (AFC) precursor provides a low energy pathway for crystallization of siderite. AFC is energetically similar to amorphous $MgCO_3$ (AMC) and more metastable than amorphous $CaCO_3$ (ACC). AMC is more persistent than either ACC or AFC, despite being more metastable. This may relate to strength of hydration.

The crystallization energetics of amorphous manganese carbonate (AMNC) has been measured by acid solution calorimetry (Radha and Navrotsky 2013). XRD studies suggest that the dry AMNC slowly crystallizes to rhodochrosite, $MnCO_3$, after 40 days. The thermal decomposition reactions of AMNC are analogous to those of AFC. In oxidative conditions, $MnCO_3$ undergoes decomposition with multiple steps and forms various high oxidation state phases such as MnO_2, Mn_2O_3 and Mn_3O_4 at different temperatures. In an inert atmosphere, it decomposes in a single step to MnO and CO_2. At higher temperature, the liberated CO_2 if not flushed out, further reacts with MnO to form Mn_3O_4 and CO. Consequently, the TG-DSC profile of AMNC in argon first shows an endothermic DSC peak (30-200 °C) corresponding to dehydration. The DSC profile for the second step (200-420 °C) shows multiple thermal events with simultaneous crystallization (exothermic) and decomposition (endothermic) occurring at ~ 400 °C. The crystallization enthalpy for freshly prepared AMNC is −32.44 ± 0.71 kJ/mol. This exothermic crystallization of AMNC suggests that the amorphous phase is metastable and could provide a low energy pathway for crystalline rhodochrosite mineralization similar to other carbonate systems with Ca, Mg and Fe cations.

The formation of common carbonates in natural environments occurs in far from equilibrium conditions and the various metastable amorphous and nanoparticulate precursor phases may control the mineralization process (Morse and Casey 1988). Calorimetric studies show that amorphous carbonate precursors provide a low energy crystallization pathway in the (Ca-Mg-Fe-Mn)-CO_3 system. To constrain the driving force for crystallization of carbonates in these systems, we compare the crystallization energetics of amorphous Ca, Mg, Fe and Mn carbonates in Table 2. The crystallization enthalpies become less exothermic with increase in

ionic radius of the cations. The ionic size driven crystallization enthalpy trend in (Ca-Mg-Fe-Mn)-CO_3 system suggests that the crystallization of amorphous phases with smaller cations may be energetically more favored than that for larger cations. A study on patterns of structure - property relationships in carbonate minerals reported many cation-size dependent phenomena in crystalline isostructural carbonates (Railsback 1999). The physical (hardness, and density) and spectroscopic (shifts in IR peak positions) properties of rhombohedral carbonates showed a linear dependency on the cation radius and degree of hydration. Such trends are mainly attributed to variation in metal-oxygen bond lengths (Railsback 1999). Geochemical properties such as solubility and distribution coefficients appear to be controlled by the degree of cationic fit in the crystal structure (Railsback 1999). The comparative study on amorphous carbonates illustrates the influence of cationic radius on thermodynamic properties of carbonate formation via crystallization processes. A critical understanding of these qualitative trends would help in developing a predictive capability for carbonate mineralization processes based on their physical properties

Nanophase carbonates and surface energies

Crystals of the same mineral grow into different shapes and morphologies under different synthetic and natural growth environments. Thermodynamic equilibrium under different conditions drives crystal growth to a minimum free energy state through wide combinations of crystal facets with different surface energies. These surface energies can be affected by the presence of inorganic, organic, and polymeric species in solution. In addition, deviations from equilibrium are common. A detailed discussion of the energetics of various carbonate crystal facets is beyond the scope of this review. When fine-grained carbonates are precipitated rapidly from aqueous solution at relatively low temperature, equilibrium among various growing faces may not be attained or maintained. The surface energies of phases can be determined by both computation and experimental techniques (see Tables 4, 5 and references therein). The computed surface energy values vary depending on the modeled crystal facet, the surface end groups, and the details of the calculation (see Table 4 and references there in). We concentrate here on surface energies measured by solution calorimetry on nanoparticle assemblages, having a range of particle sizes but a well-defined average surface area and showing some average distribution of exposed crystal faces determined by the precipitation conditions. Such materials may in fact be representative of many natural precipitation environments.

Calorimetric studies have demonstrated that nanoscale intermediates can control phase formation and morphology by reversing the order of thermodynamic stability of polymorphs (Navrotsky 2004, 2009, 2011). These size induced crossovers in the free energies of the polymorphs at the nanoscale show a correlation between increasing metastability and decreasing surface energy (Navrotsky 2001, 2004). The free energy crossovers due to increasing specific surface area (decreasing particle size) combined with small energy differences between bulk polymorphs have been exhibited by several oxide systems including alumina, titania, zirconia iron oxides and manganese oxides (McHale et al. 1997; Ranade et al. 2002; Pitcher et al. 2005; Levchenko et al. 2006; Navrotsky et al. 2008, 2010; Radha et al. 2009).

Calcium carbonate exists in five different crystalline polymorphs at ambient pressure as calcite, aragonite, vaterite (anhydrous phases), monohydrocalcite and ikaite (hydrated phases), in addition to various amorphous forms. Thermodynamic stability crossovers in calcium carbonate system at nanoscale regimes would have tremendous geologic and technological implications, including geological sequestration of CO_2. Calcium carbonate precipitation in a geologic CO_2 repository occurs in confined micro/nanopores of the sandstone aquifer and the stability crossovers could alter the dominant calcium carbonate phase precipitated under such conditions. Also the influence of the increased pressures, temperatures, and ionic strength of the environment could alter the precipitation pathway.

Table 4. A summary of computed calcite surface energies. Reproduced with permission from Forbes et al. (2011). Copyright © 2011 Elsevier Science.

Calcite Crystal Face	Energy of hydrous surface (J/m^2)	Energy of anhydrous surface (J/m^2)	Reference
$10\bar{1}4$	0.288	0.86	Kvamme et al. (2009)
	0.232	0.863	Hwang et al. (2001)
	0.387	0.59	Kerisit et al. (2003)
	0.14	0.60	Duffy and Harding (2004)
	0.16	0.59	de Leeuw and Parker (1998)
		0.59	Titloye et al. (1998)
$10\bar{1}0$	0.778	1.50	Kvamme et al. (2009)
		1.37	Hwang et al. (2001)
		0.95	Kerisit et al. (2003)
		1.23	Titloye et al. (1998)
	0.75	0.97	de Leeuw and Parker (1998)
		0.97	Titloye et al. (1998)
$10\bar{1}2$	0.37 or 0.44*	1.06 or 1.25*	Duffy and Harding (2004)
		0.75 or 1.06*	Bruno et al. (2008)
		2.62	Braybrook et al. (2002)
		2.65	Massaro et al. (2008)
$11\bar{2}0$		1.39	Titloye et al. (1998)
	0.43	1.39	de Leeuw and Parker (1998)

* The lower value corresponds to a surface terminated by carbonate groups and the higher value is a surface terminated by calcium ions.

Table 5. A summary of measured calcite surface energies by different experimental methods. Reproduced with permission from Forbes et al. (2011). Copyright © 2011 Elsevier Science.

Surface energy (J/m^2)	Method	Reference
0.085	Homogeneous nucleation	Sohnel and Mullin (1982)
0.064	Heterogeneous nucleation	Lioliou et al. (2007)
0.032-0.035	Heterogeneous nucleation on polymers	Dousi et al. (2003), Gomez-Morales et al. (2010)
0.033	Heterogeneous nucleation	Manoli and Dalas (2002)
0.23	Cleavage experiments	Gilman (1960)
0.347 ± 0.045	Cleavage technique	Gupta and Santhanam (1969)
0.32	Subcritical cracking	Roayne et al. (2011)
0.098	Contact angle measurements	Janczuk et al. (1986)
0.072	Contact angle measurements	Okayama et al. (1997)
0.54-0.76	Heat of immersion	Goujon and Mutaftschiev (1976)
0.762 ± 0.002	Heat of immersion	Wade and Hackerman (1959)

Surface energy data for calcite by both experimental and computational methods show a wide distribution covering several orders of magnitude (see Tables 4 and 5). Generally, calculated surface energies for other oxides agree with the measured values within 10-50%. Computed values are based on the ideal surface, while real surfaces have complex and heterogeneous structures with edge sites and defects (Navrotsky 2009, 2011). It is possible that the less directly determined experimental surface energy values for calcite are low because they are derived based on classical homogeneous and heterogeneous nucleation theory, rather than measured directly (see Table 5). The initial solid formed may be different (e.g. prenucleation clusters leading to amorphous precipitates). The surface energy of such metastable precursor phases (ACC or vaterite) are expected to be lower than that of the stable calcite phase. Furthermore, the induction times used in the surface energy determinations may not correspond to those for the formation of calcite. A similar concern was raised earlier in deriving the interfacial surface tension of calcite based on nucleation experiments (Christoffersen et al. 1991).

To determine the effect of particle size on thermodynamic stability in carbonate systems, the energetics of nanophase calcite and nanophase manganese carbonate phases were measured by acid solution and water adsorption calorimetric techniques (Forbes et al. 2011; Radha and Navrotsky 2013). A critical assessment of three different characterization techniques (XRD, TEM and BET methods) for particle size analysis for calcite phases suggests that the surface area measurement using the BET method is best suited for use in surface energy determination of calcite type structures (Forbes et al. 2011). The enthalpies of solution (ΔH_{sol}) for the nanophase and bulk carbonate phases were measured by acid solution (5 M HCl) calorimetry. The surface energy for a given surface area is the excess enthalpy of nanophase with respect to bulk obtained after subtracting the contribution of adsorbed water from enthalpies of solution (ΔH_{soln}) and can be written as

$$\Delta H_{\text{sol-bulk}} = \Delta H_{\text{sol-corr nano}} + \text{SA} \times \gamma$$

where SA = surface area of nanocalcite (m^2/mol); γ = surface enthalpy (J/m^2)

Solution enthalpies are corrected for physically ($\Delta H_{\text{sol-corr-physi}}$) or chemisorbed ($\Delta H_{\text{sol-corr-chemi}}$) water contents and plotted against the surface area obtained from BET analysis. The negative of the slopes of the linear fits give the surface enthalpies for hydrous and anhydrous surfaces. These surface enthalpy values are good approximations to the surface energy and surface free energy (surface tension) since the contribution of excess volume (*PV* term) and surface entropy ($T\Delta S$ term) are expected to be small (Navrotsky 2009). Figure 12 shows surface energy plots of hydrous and anhydrous surfaces of nanophase calcite and manganese carbonate. From the calorimetric data, the surface energies of hydrous and anhydrous surfaces are 1.48 ± 0.21 and 1.87 ± 0.13 J/m^2 for calcite (Forbes et al. 2011) and 0.64 ± 0.08 J/m^2 and 0.94 ± 0.12 J/m^2 for nano manganese carbonate (Radha and Navrotsky 2013). The measured values are generally larger than predicted from computational models (0.14 to 0.77 J/m^2 for hydrous and 0.59 to 2.65 J/m^2 for anhydrous surface) for idealized calcite surfaces (de Leeuw and Parker 1998; Titloye et al. 1998; Hwang et al. 2001; Braybrook et al. 2002; Kerisit et al. 2003; Duffy and Harding 2004; Bruno et al. 2008; Massaro et al. 2008; Kvamme et al. 2009) probably because the synthetic samples contain a range of planes and defect structures.

Studies of surface energies for aragonite and vaterite phases are in progress. Given the small differences in energy between the polymorphs, there is a good possibility that stability crossovers of the nanoscale may exist for calcium carbonate system as well as for oxide minerals.

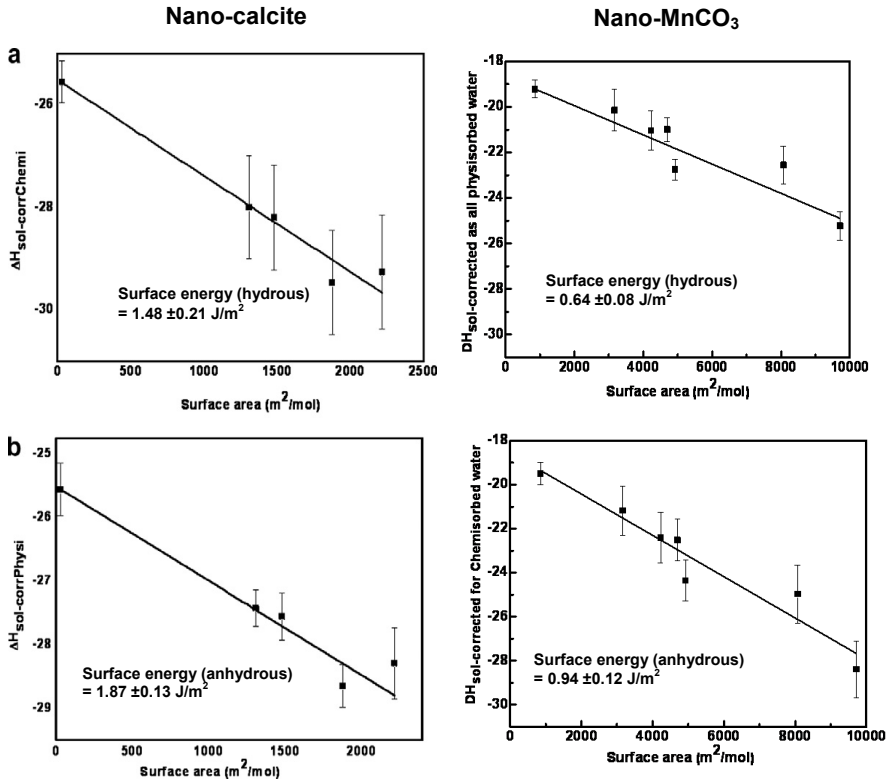

Figure 12. Surface energy plots of hydrous and anhydrous surfaces of nanophase calcite and manganese carbonate phases. Reprinted with permission of Elsevier Science from Forbes et al. (2011). Copyright © 2011 Elsevier Science.

CRYSTALLINE DIVALENT CARBONATES

Thermodynamics of rhombohedral and orthorhombic carbonates

Crystalline anhydrous metal carbonates, M(II)CO_3 exist either in rhombohedral (calcite type) or orthorhombic (aragonite-type) structure depending on the cation size (Reeder 1983). Divalent cations smaller than Ca^{2+} form rhombohedral carbonates with six coordinated cations, whereas cations bigger than Ca^{2+} crystallize in the orthorhombic aragonite structure with nine coordinated cations. Ca^{2+} has an intermediate size and exists in both structural forms as calcite and aragonite in addition to a hexagonal vaterite phase (Reeder 1983; Ribbe et al. 1987). The calcite-type rhombohedral structure consists of alternate layers of Ca atoms (A) and carbonate ions (B/C) (Fig. 13). The flat carbonate ions in successive layers stack in reverse (ABAC) orientation to facilitate octahedral co-ordination of cation with six oxygens from different carbonate anions. Consequently, the rhombohedral unit cell parameter along the stacking direction is the height of six layers of carbonate ions. In the aragonite-type orthorhombic carbonate structure; the layer stacking is pseudohexagonal due to nonplanar metal layers having out of plane cation displacements (around ± 0.005 nm) and corrugated carbonate layers with reverse orientations (Speer 1983). This facilitates the formation of 9-coordinated metal cations having six M-O bonds with oxygens at the edges of 3 carbonate groups and three M-O bonds with three corner oxygens from three separate carbonate groups (see Fig. 13).

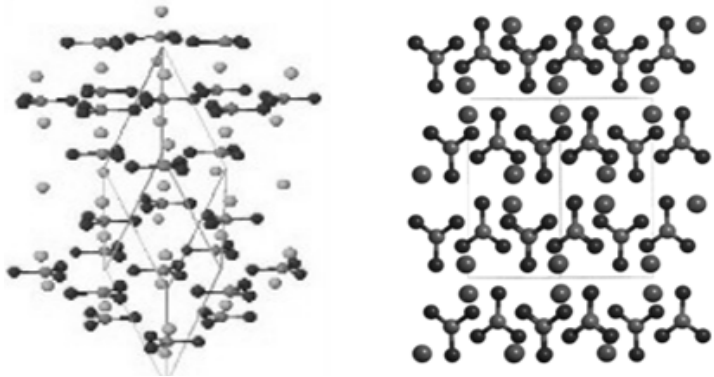

Figure 13. The crystal structures of rhombohedral (calcite-type) and orthorhombic (aragonite-type) carbonates. From *http://www.crystal.unito.it/prtfreq/jmol.html*.

Figure 14 shows the free energy and the solubility data for some common divalent metal carbonate minerals as a function of cation radius (Railsback 1999). For rhombohedral carbonates, the thermodynamic stability generally increases (the free energy of formation from ions at 25 °C becomes more exothermic) with increase in cation radius, although calcite is an exception. The most common rhombohedral minerals, calcite (with largest cation, Ca^{2+}) and magnesite (smaller Mg^{2+} cation) have lower stability and hence are more soluble. The orthorhombic carbonates show a similar trend with phases having intermediate radius being thermodynamically more stable than the end members of the series, aragonite ($CaCO_3$) and witherite ($BaCO_3$). This trend in thermodynamic stability seems to have direct structural correlation with the cation coordination geometries. The distorted 6-fold and 9-fold coordination geometries due to poor fit of largest and smallest cations in the rhombohedral and orthorhombic structures lower the thermodynamic stability. The most abundant sedimentary carbonate minerals calcite ($CaCO_3$), aragonite ($CaCO_3$), magnesite ($MgCO_3$) and dolomite ($CaMg(CO_3)_2$) fall into the lower stability region relative to aqueous solution and hence are more reactive. The large cation aragonite carbonates are far less soluble. The ordered mixed cation carbonates, dolomite [$CaMg(CO_3)_2$], ankerite [$Ca(Fe,Mg,Mn)(CO_3)_2$] and alstonite [$BaCa(CO_3)_2$] are more stable than their respective end members.

Calcite-aragonite phase transition at high pressure and orientational disordering in calcite at high temperature

The calcite-aragonite equilibrium is temperature and pressure dependent and has been studied extensively due to its importance in petrology and geo-thermobarometry (Carlson 1983; Essene 1983). Though these phenomena become important at pressures and temperatures above those envisioned for CO_2 sequestration, they shed light on issues of structure and bonding relevant to carbonate behavior. Pressure extends the carbonate stability field to higher temperature by disfavoring CO_2 evolution. The pressure-temperature *(P-T)* calcite-aragonite equilibrium curve calculated using thermodynamic data from both direct and indirect free energy measurements (Redfern et al. 1989) shows a significant change in slope between low and high *P-T* regimes (see Fig. 15). These changes were initially attributed to a first-order phase transition within the calcite phase (Cohen and Klement 1973). However, comprehensive structural studies by high temperature XRD and neutron scattering indicated gradual orientation disordering in calcite leading to $R\bar{3}c$ *to* $R\bar{3}m$ transition (Markgraf and Reeder 1985; Dove and Powell 1989).

A combined low temperature heat capacity and high-temperature transposed-temperature drop calorimetric study has been used to measure the energetic change associated with the

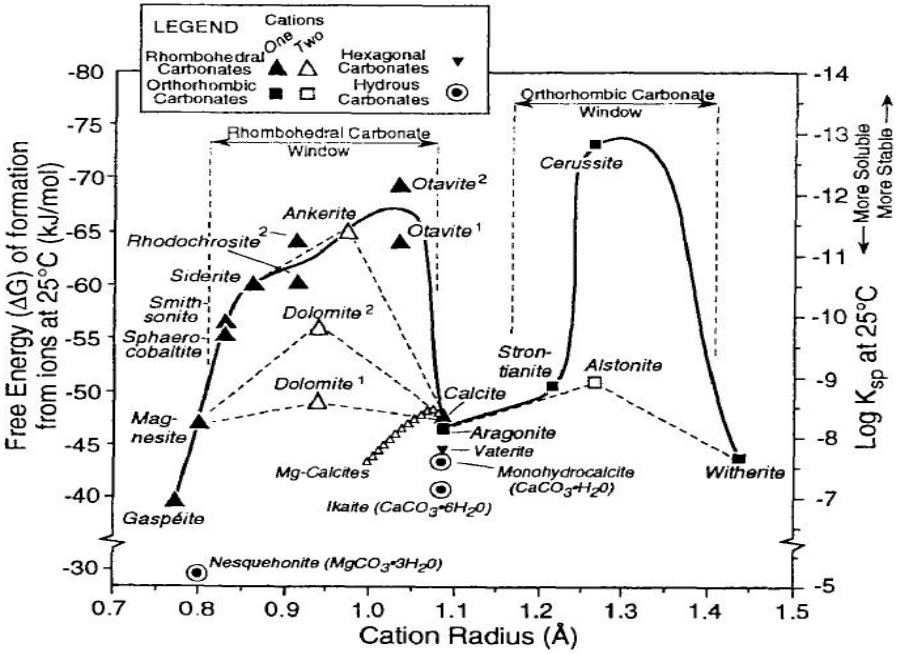

Figure 14. The free energy and the solubility data for common divalent metal carbonate minerals as a function of cationic radius. K_{sp} is the solubility product, and represents the equilibrium constant for dissolution or precipitation. Originally published in Railsback (1999) and reprinted with permission. Copyright © 1999 by Springer Science.

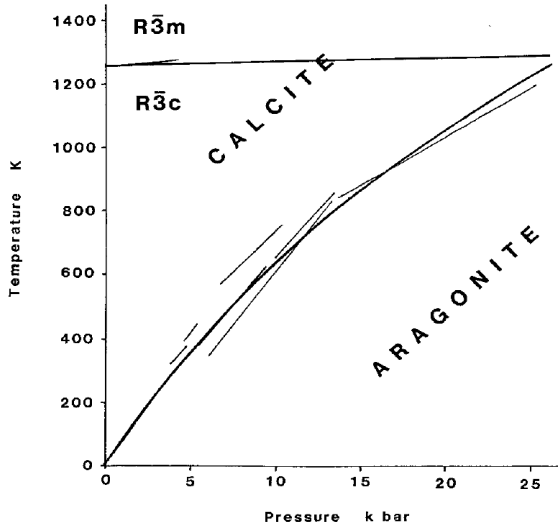

Figure 15. The phase diagram of calcite-aragonite. Thick lines are the phase boundary calculated for the $R\bar{3}c$ to $R\bar{3}m$ disorder transition and thin lines are the experimental data (Jamieson 1953; Simmons and Bell 1963; Crawford and Fyfe 1964; Johannes and Puhan 1971; Zimmermann 1971; Cohen and Klement 1973; Irving and Wyllie 1973). Reprinted from Redfern et al. (1989) with permission. Copyright © 1989 by Springer Science.

orientational order-disorder transition in order to understand its implication for the calcite/aragonite phase boundary behavior (Redfern et al. 1989). The deviation of the calorimetrically measured enthalpy of high temperature calcite phase ($R\bar{3}m$) between 973 K and 1325 K from the extrapolated low temperature phase ($R\bar{3}c$) heat capacity data gives the enthalpy for the orientational order-disorder transition (6.9 ± 1.1 kJ/mol) (Fig. 16). The calculated phase diagram based on excess enthalpy analyzed by Landau theory for tricritical phase transition is in agreement with the experimental observations. This supports the change in slope of the calcite/aragonite phase boundary is due to the $R\bar{3}c$ to $R\bar{3}m$ transition in calcite.

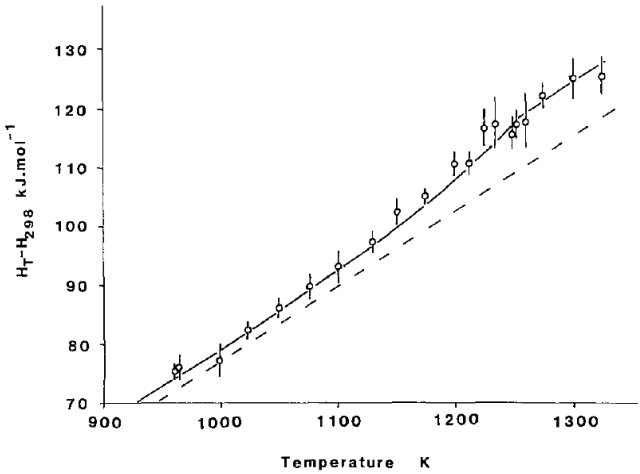

Figure 16. Calorimetric data for the enthalpy of calcite between 900 K and 1350 K (solid line) plotted with extrapolated low temperature heat capacity (dashed line) data from Jacobs et al. (1981). Taken from Redfern et al. (1989) with permission. Copyright © 1989 by Springer Science.

Vaterite

Vaterite is thermodynamically the least stable anhydrous polymorph of calcium carbonate under ambient conditions and is generally found in low temperature environments: biological systems, sediments, cements and as an intermediate phase during calcite synthesis (Plummer and Busenberg 1982; Mann et al. 1988; Friedman et al. 1993; Falini et al. 1998; Friedman 2005; Hu et al. 2010; Natoli et al. 2010). Vaterite transforms to calcite at room temperature on aging and on heating at 693-753 K. However, biomolecules or organic additive templates are shown to stabilize synthetic vaterite under ambient conditions (Pach et al. 1990; Kanakis and Dalas 2000; Kanakis et al. 2001; Lee et al. 2005; Han et al. 2006; Pouget et al. 2010). It is not clear whether such stabilization is purely kinetic or has a thermodynamic basis arising from adsorption of organics. Most vaterite samples are very fine grained (nanophase). There are reports of at least three different types of vaterite structures, (a) disordered hexagonal ($P6_3/mmc$), (b) ordered superstructures (P_6522) and (c) ordered orthorhombic (*Pbnm)* as shown in Figure 17 (Kamhi 1963; Medeiros et al. 2007; Wang and Becker 2009, 2012; Ren et al. 2013).

The hexagonal structure of vaterite has alternate layers of Ca ions and carbonate ions similar to rhombohedral carbonates. However the carbonate layers in vaterite are disordered with CO_3 planes orienting perpendicular to the 001 stacking direction. The presence of stacking faults and their ordering in the (001) plane could lead to superstructure formation. The formation of such superstructure established from *ab initio* calculations and molecular-dynamics (MD)

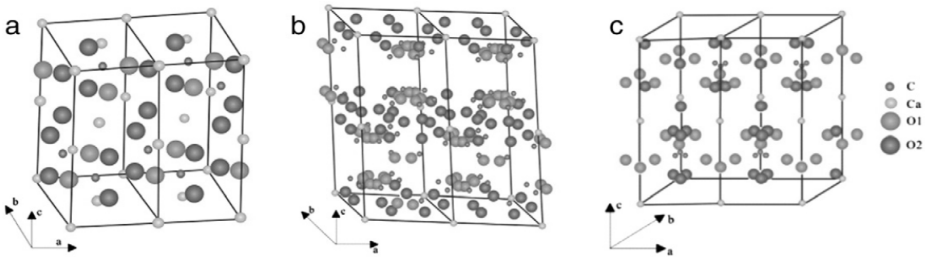

Figure 17. Vaterite models with (a) rhombic (b) hexagonal and (c) ordered hexagonal crystal structures. Reproduced with permission from Ren et al. (2013). Copyright © 2013 Elsevier Science.

simulations (Wang and Becker 2009) is found to be consistent with NMR results (Michel et al. 2008). The ordered orthorhombic structure was proposed recently based on X-ray diffraction data and is 3 to 10 kJ/mol higher than calcite, and the experimentally measured values fall within the computed range (3.4 kJ/mol, (Wolf et al. 1996, 2000) and 6.2 kJ/mol (Plummer and Busenberg 1982). A possible reason for this difference in experimental values could be the existence of a variable degree of disorder in the experimental samples. The computed enthalpy of disordered vaterite is 11-14 kJ/mol above that of ordered vaterite and 16-21 kJ/mol higher than calcite (Wang and Becker 2009, 2012 and also see Table 3). In contact with aqueous solution, the initial vaterite phase is thought to evolve from an amorphous precursor (ACC) phase with orientationally disordered carbonate ions. The degree of disordering in vaterite seems to have a large effect on the relative stability of vaterite with respect to ACC, aragonite, and calcite as indicated by large differences in their energetics. The energy differences among the three ordered crystalline polymorphs (ordered vaterite, aragonite, and calcite) are found to be small (Plummer and Busenberg 1982; Wolf et al. 1996, 2000; Wang and Becker 2009, 2012; Raiteri et al. 2010). Small energy differences between ACC and disordered vaterite are also predicted (Koga et al. 1998; Wolf and Gunther 2001; Radha et al. 2010; Wang and Becker 2009, 2012) (Fig. 18).

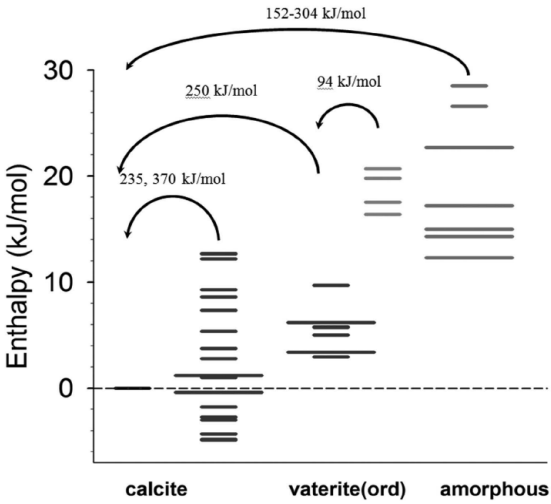

Figure 18. Enthalpies and activation energies for phase transitions among different calcium carbonate polymorphs with respect to calcite as reference (thin dashed line). Long, thick lines are experimental values, short, thick lines are theoretical calculations and the curved lines with arrows are the activation energy of the transition. Reproduced with permission from Wang and Becker (2012).

BINARY DIVALENT METAL CARBONATE SYSTEMS

The binary carbonate systems (MCO_3-NCO_3) form solid solutions with calcite, orthorhombic and dolomite structures. They are completely or partially miscible. The miscibility depends on the differences between the cation sizes of the end members of the binary system for calcite-type structures (see Table 6) and on the temperature of formation. Thermodynamics of formation and mixing properties determines the phase formation in these binary systems. Calorimetric measurements of energetics have revealed interesting mixing behavior in some of the binary carbonate systems and are discussed below.

Table 6. Cation size differences between the end members of the binary system Reproduced with permission from Reeder (1983).

Complete miscibility cation pairs		Limited miscibility cation pairs	
M^{2+} - N^{2+}	Δr (nm) in VI coordination	M^{2+} - N^{2+}	Δr (nm) in VI coordination
Fe - Mg	0.006	Ca - Mg	0.028
Ca - Cd	0.005	Ca - Fe	0.022
Mg - Co	0.003	Ca - Mn	0.017
Fe - Mn	0.005	Cd - Mg	0.023
Mg - Mn	0.011	Ca - Co	0.026
		Ca - Ni	0.031

$CaCO_3$-$MgCO_3$

$CaCO_3$-$MgCO_3$ is an important binary system in several geochemical settings involving sedimentary, metamorphic, marine, and mantle processes as well as in biological systems (Bischoff et al. 1983; Mackenzie et al. 1983). This binary system has limited miscibility with disordered rhombohedral $CaCO_3$-$MgCO_3$ solid solution interrupted by the dolomite phase field around the midpoint composition and a miscibility gap in both the Mg-rich and Ca-rich regions (see Fig. 19) (Graf and Goldsmith 1955; Goldsmith and Heard 1961; Bischoff et al. 1983; Mackenzie et al. 1983; Walter and Morse 1984).

Calorimetric studies of magnesian calcite and calcian dolomite have shown different energetic trends (Navrotsky and Capobianco 1987). In the Ca-rich region, Mg substitutes up to 25 mol% $MgCO_3$ to form calcite-type solid solution in low-temperature inorganic and biogenic environments. The biogenic magnesian calcites seem to have greater local disorder and show subtle differences in their crystallographic parameters and vibrational spectra compared to their synthetic analogues (Bischoff et al. 1983). Several studies on magnesian calcites have reported lowering of stability and increase in reactivity with increase in Mg substitution (Bischoff et al. 1983; Mackenzie et al. 1983; Navrotsky and Capobianco 1987; Busenberg and Plummer 1989). However, the calorimetric measurements on synthetic magnesian calcites, $Ca_{1-x}Mg_xCO_3$ for $x < 0.12$ show a small exothermic enthalpy of mixing (see Fig. 20) as opposed to the expected destabilization (hence positive heats of mixing) due to cation size mismatch (Navrotsky and Capobianco 1987; Chai et al. 1995). Gordon and Greenwood (1970) suggested positive deviations from ideal activity-composition relations and hence positive deviations in free energies at high temperature near 700 °C. The combination of positive excess free energies and negative enthalpy of mixing suggest the negative excess entropy of mixing for this system. This could probably associated with some sort of structural ordering such as clustering of Mg that produces a favorable lowering of the enthalpy but a loss of entropy in synthetic magnesian calcites equilibrated at 700 °C. The random stacking of Mg-

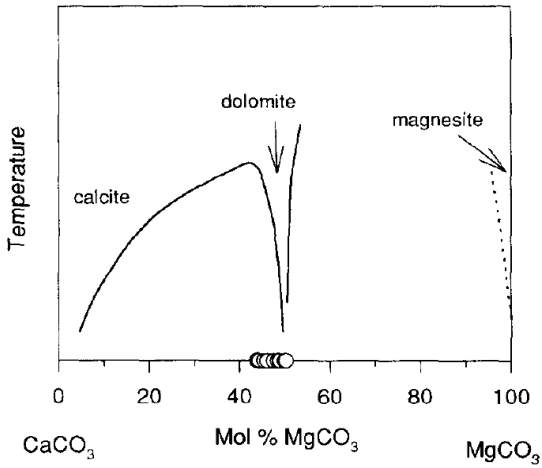

Figure 19. Schematic of $CaCO_3$-$MgCO_3$ *T-X* diagram with open circles showing the Ca-rich dolomite region after Goldsmith and Heard (1961). Reprinted with permission from University of Chicago Press, USA. Copyright © 1961, University of Chicago.

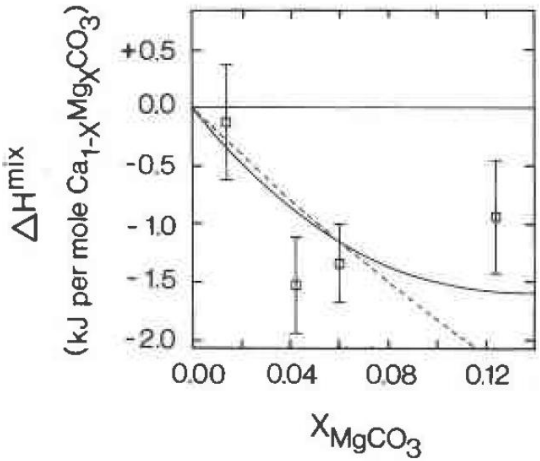

Figure 20. Enthalpy of mixing calculated from calorimetric data in magnesiacn calcites ($Ca_{1-x}Mg_xCO_3$) with a data fit using ideal mixing with equations $\Delta H_{mix} = X(1-X)\,(-20.37 \pm 13.39)$ (solid line) and $\Delta H_{mix} = X\,(1-X)\,[-25.65 \pm 5.94 + (88.49 + 49.71)X]$ (dashed line). Reprinted with permission from Navrotsky and Capobianco (1987).

rich layers between Ca layers rather than random substitution of Mg for Ca could also lead to energetically stable Mg-calcites.

$FeCO_3$-$MgCO_3$

The mixing of Fe^{2+} and Mg^{2+} cations in octahedral sites is a common occurrence in sedimentary and metamorphic carbonate minerals. For $FeCO_3$-$MgCO_3$, the mixing property studies suggest the formation of a complete solid solution (Rosenberg 1963; Davidson 1994). The enthalpy of mixing for this system has been obtained by a two-step calorimetric method at 770 °C (Chai and Navrotsky 1996b). In the first step, sample was decomposed in an oxygen atmosphere and in the second step; the decomposed products (a mixture of $MgFe_2O_4$, spinel and MgO or hematite) were dissolved in lead borate solvent in air. The enthalpies of mixing for the $FeCO_3$-$MgCO_3$ system are slightly positive due to a slight mismatch in Fe^{2+} and Mg^{2+} sizes. Fitting

experimental data with a regular solution model ($\Delta H_{mix} = WX_{Fe}X_{Mg}$, where W = the interaction parameter, and X_{Fe} and X_{Mg} = mole fractions of $FeCO_3$ and $MgCO_3$ in the solid solution) gives the interaction parameter W as 4.44 ± 0.75 kJ/mol (see Fig. 21).

The positive deviation of enthalpy from ideal mixing is a signature of probable low temperature exsolution. The phase diagram of $FeCO_3$-$MgCO_3$ is derived from the Gibbs free energy of mixing by using a regular solution model and the ideal entropy of mixing (see Fig. 22). The miscibility gap and the spinodal curve suggest the complete solid solution in all geological environments for $MgCO_3$-$FeCO_3$ system with possible exsolution at a very low critical temperature of about 267 K (Chai and Navrotsky 1996b).

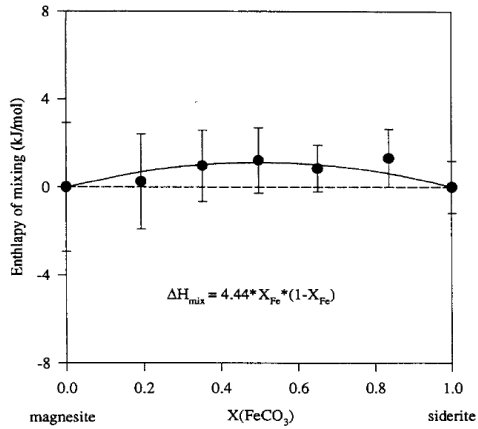

Figure 21. Enthalpy of mixing for the $FeCO_3$-$MgCO_3$ system with a fit using a regular solution parameter of 4.44 kJ/mol (solid line) and the dashed line is for ideal mixing. Reprinted with permission from Chai and Navrotsky (1996b). Copyright © 1996 Elsevier Science.

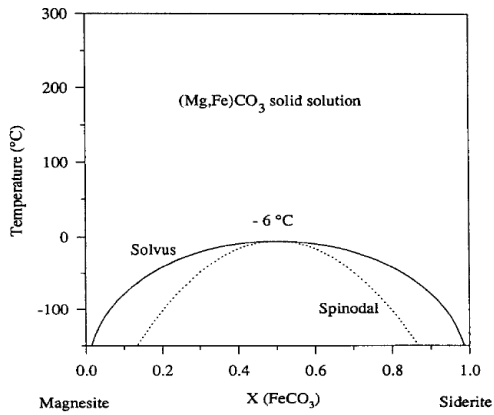

Figure 22. Calculated phase diagram of the $FeCO_3$-$MgCO_3$ system showing the solvus (solid curve) and the spinodal (dashed curve). Reprinted from Chai and Navrotsky (1996b) with permission. Copyright © 1996 Elsevier Science.

$CaCO_3$-$MnCO_3$

The $CaCO_3$-$MnCO_3$ (calcite-rhodochrosite) binary system is a part of the rock-forming carbonate tetrahedron, but such carbonates are often found in association with other Mn and Ca minerals. The minerals of this system, Mn-bearing calcites and kutnahorite with dolomite-type structure are found in deep-sea sediments (Pedersen and Price 1982). Thermodynamic studies by phase equilibrium and calorimetric methods showed positive excess free energies (see Fig. 23) and complex endothermic and exothermic enthalpies of mixing (see Fig. 24), which suggest negative excess entropies of mixing supporting short range ordering (Goldsmith and Graf 1957; De and Peters 1981; Capobianco and Navrotsky 1987). For phase equilibrium calculations, the $(Ca,Mn)CO_3$ decomposition and Gibbs-Duhem relation were used to obtain the activity coefficients of $MnCO_3$ (γ_{MnCO3}) and $CaCO_3$ (γ_{CaCO3}) as a function of composition X. The excess free energy of mixing at 700 °C is found to be positive (Fig. 23) and the enthalpy of mixing is asymmetric at 600 °C (Fig. 24). Addition of $MnCO_3$ destabilizes the calcite and $CaCO_3$ addition results in exothermic mixing with rhodochrosite without any kutnahorite as this temperature is above its stability field. This again supports negative excess entropies of mixing. The calculated and the experimentally determined solvi (De and Peters 1981) for this system are shown in Figure 25. The metastable solvus closes at 355 °C, whereas the experimental solvus extends to about 550 °C. The suppression of kutnahorite

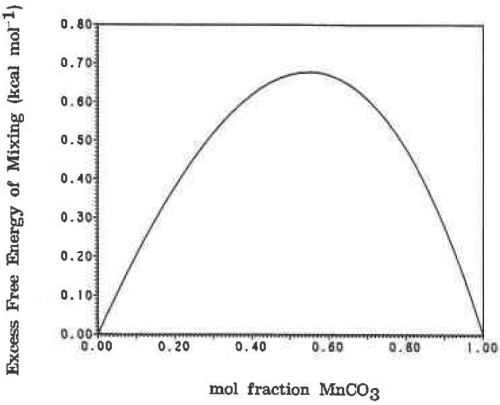

Figure 23. Excess free energy for the calcite-rhodochrosite system as a function of composition at 700 °C. Reproduced with permission from Capobianco and Navrotsky (1987).

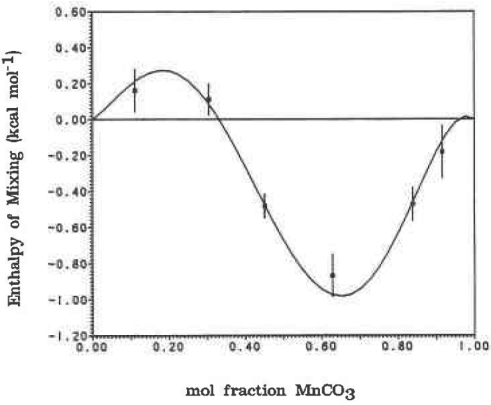

Figure 24. Calorimetric data for 600 °C samples with least-square fit to the data. Reproduced with permission from Capobianco and Navrotsky (1987).

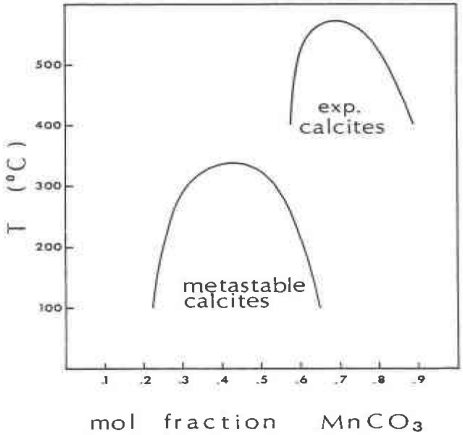

Figure 25. Phased diagram of calcite-rhodochrosite with experimental solvus (De and Peters 1981) and metastable solvus calculated from temperature-dependent excess-free-energy functions. Reproduced with permission from Capobianco and Navrotsky (1987).

phase formation increases the solid solubility in this system.

$CaCO_3$-$SrCO_3$

The $CaCO_3$-$SrCO_3$ system is an important component of solid-aqueous phase interactions in geochemistry and relevant for contaminant of migration (including that of radium) in the environment (Plummer and Busenberg 1987; Koenigsberger and Gamsjager 1990; Plummer et al. 1992). This system crystallizes in the orthorhombic aragonite structure. Thermodynamic data have been determined by solubility studies (Holland et al. 1963; Plummer et al. 1992) electrochemical (Casey et al. 1996b) and calorimetric measurements (Casey et al. 1996a). The calorimetric measurements show positive heats of mixing (ΔH_{mix}) with a positive symmetric deviation that reaches a maximum value of 3.82 ± 0.94 kJ/mol at x = 0.5 (see Fig. 26). The ΔG_{mix} (0.0 < x < 0.9) of mixing for $Ca_{(1-x)}Sr_xCO_3$ solid solution by electrochemical measurements also shows a similar positive trend (+3.0 ± 1.6 kJ/mol at x = 0.7), which suggest small or zero excess entropy of mixing for this system (see Fig. 26).

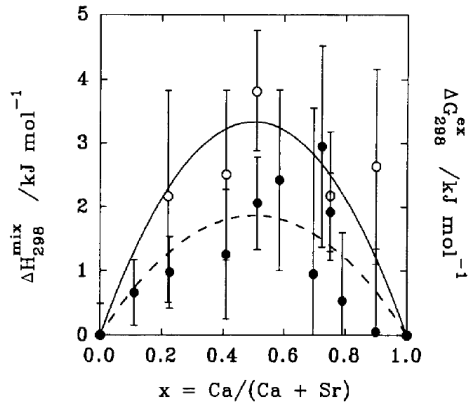

Figure 26. The ΔH_{ds} values from calorimetric data (solid line) and ΔG_{excess} data from Casey et al. (1996b) (dashed line) with fits using the regular-solution model. Reprinted with permision from Casey et al. (1996a). Copyright © 1996 Elsevier Science.

Therefore a regular solution model, $\Delta H_{mix} = Wx\ (1 - x)$ was used to obtain the interaction parameter (W = 13.5 ± 1.3 kJ/mol) for this system (see Fig. 27). The large interaction parameter suggests very limited miscibility at ambient temperature. But in nature, aragonites having l-2 mol% $SrCO_3$ (a few to 14% $SrCO_3$) and strontianites with 25-30 mol% $CaCO_3$ have been observed (Plummer and Busenberg 1987; Koenigsberger and Gamsjager 1990; Plummer et al. 1992; Casey et al. 1996a). The formation of such phases has been attributed to metastable equilibrium of minerals with aqueous solution.

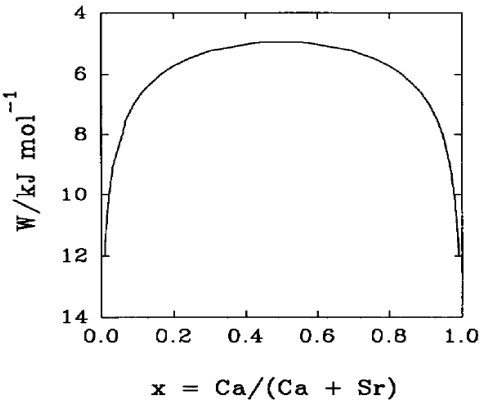

Figure 27. The stable compositions of orthorhombic Sr-CO_3-$CaCO_3$ system at 298 K and 1 bar as a function of the interaction parameter for a regular solution. Reprinted from Casey et al. (1996a) with permission. Copyright © 1996 Elsevier Science.

Dolomite-type structures and energetics of order-disorder phenomena

Dolomite (space group $R\bar{3}$) is a superstructure of calcite or magnesite (space group $R\bar{3}c$) having ordered alternate calcium and magnesium layers. In $CaMg(CO_3)$, the average Ca-O distance is 2.390 Å and Mg-O distance is 2.095 Å (Wyckoff 1964) and this difference in bond length drives the formation of the ordered structure. The ideal composition of dolomite contains

50 mol% each of Ca and Mg carbonates. However, in nature Ca rich dolomite having up to 57-58 mol% of $CaCO_3$ are common (Lumsden and Chimahusky 1980; Sperber et al. 1984; and references therein). Mg rich dolomites are rare and limited to less than 1 mol% from the ideal composition. High temperature experimental studies have reported the existence of dolomite having 5-6 mol% excess $CaCO_3$ with substitutional cation disorder at 900-1100 °C (Goldsmith and Graf 1958; Goldsmith 1967; Reeder 1983; Reeder and Sheppard 1984; Navrotsky and Capobianco 1987). Cation ordering is favored at lower temperature (Reeder and Markgraf 1986) and above 1150 °C dolomite transforms to calcite structure with a largely disordered distribution of Ca and Mg.

The more endothermic enthalpies of formation of Ca-rich dolomites with increase in $CaCO_3$ content indicate that these phases are thermodynamically unstable (see Fig. 28). The substitution of Ca for Mg in the Mg layer of dolomite is energetically unfavorable. This is further supported by thermodynamic cluster variation model calculations that show positive contribution to the enthalpy from interactions within layers and a negative contribution from interactions between layers in the dolomite structure (Burton 1987; Capobianco et al. 1987). Therefore the formation of Ca-rich dolomite in sedimentary environments seems to be controlled more by kinetics than by thermodynamics.

The different trends in formation energetics of magnesian calcite and dolomite solid solutions are shown together in Figure 29 (Chai et al. 1995; Chai and Navrotsky 1996b). The magnesian calcites show a small negative deviation from the mechanical mixtures of stoichiometric dolomite and calcite, as well as a negative heat of mixing between $CaCO_3$ and $MgCO_3$. For calcian dolomites, the formation enthalpies deviate positively from the mechanical mixture to a larger extent. This behavior is related to ionic radii or bond lengths and attributed to energetically more favorable substitution of a smaller Mg cation for a larger Ca in magnesian calcite than of a larger Ca for a smaller Mg in calcian magnesite. However, formation of Mg-rich dolomite seems to be more complicated, involving cation order-disorder and mixed-layer sequences.

$CdCO_3$-$MgCO_3$

This system is considered an analogue for $CaCO_3$-$MgCO_3$, with disordering occurring at lower temperature. The dolomite type phases in $CdCO_3$-$MgCO_3$ system showed different degrees of ordering on quenching at different pressure and temperature (0.1-1 gPa pCO_2 and 600-850 °C). The structures of these phases are well constrained since a large difference in atomic number between Cd and Mg makes it easier to characterize site occupancies by XRD. The completely ordered structure forms at 600 °C and disordered samples form at 800 °C, while the samples with intermediate ordering at 750-775 °C. The calorimetric data of Cd-Mg dolomite type solid solution for samples quenched from 600 to 850 °C has been reported (Capobianco et al. 1987). The enthalpy of formation of ordered $CdMg(CO_3)_2$ from $CdCO_3$ and $MgCO_3$ is -5.6 ± 0.8 kJ/mol; that of the disordered phase is $+8.1 \pm 0.8$ kJ/mol. The long-range order parameter changes from unity to zero in this range and the enthalpy of disordering is 13.7 ± 0.8 kJ/mol. The $CdCO_3$-$MgCO_3$ binary phase equilibrium also has two regions comprising disordered calcite-type and dolomite type solid solutions similar to $CaCO_3$-$MgCO_3$ system. The relationship between the structure and energetics associated with order-disorder phase transformation and phase equilibrium in $CdCO_3$-$MgCO_3$ has been studied by different structural models and is compared with the experimental data. The experimentally determined order-disorder transition is sharper with a narrower temperature range than predicted from the models. (Capobianco et al. 1987). The phase diagrams based on different thermodynamic models produce a reasonably good fit with the data from different experiments with a stability field for two disordered phases.

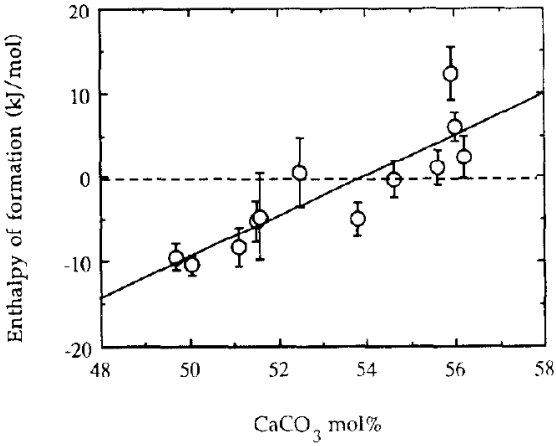

Figure 28. Enthalpies of formation of Ca-rich dolomite with the best fit for the data as a solid line. Reprinted with permission from Chai et al. (1995). Copyright © 1995 Elsevier Science.

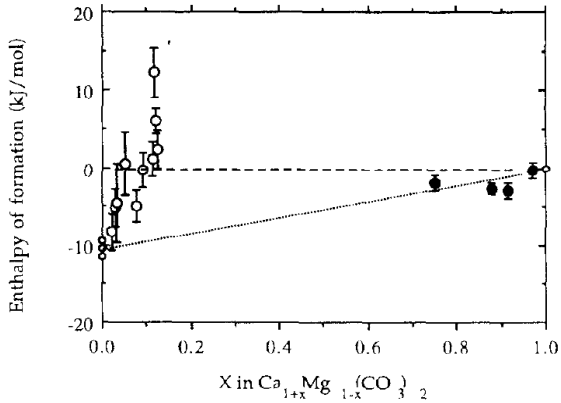

Figure 29. Enthalpy of formation of Ca-rich dolomite (open circles) and magnesian calcite (filled circles) and the small open circles for stoichiometric dolomite and calcite. Reprinted with permission from Chai et al. (1995). Copyright © 1995 Elsevier Science.

$CaMg(CO_3)_2$ - $CaFe(CO_3)_2$ solid solution (dolomite - ankerite join)

Though there is no report of occurrence of pure ordered calcium iron carbonate, ankerite, $CaFe(CO_3)_2$, but dolomite structured solid solution ($Ca(Fe_xMg_{1-x})(CO_3)_2$, $0 \le x \le 0.7$) formed by partial substitution of Fe in Mg sites of dolomite is common in nature (Reeder 1983; Reeder and Dollase 1989; Davidson et al. 1993 and references therein). However, there are reports of existence of synthetic disordered $CaFe(CO_3)_2$ with calcite-type structure at 845 °C and 3 gPa, indicating the possibility of existence of an ordered $CaFe(CO_3)_2$ phase at lower temperature (Davidson et al. 1993).

The calorimetrically measured enthalpy of formation of disordered $CaFe(CO_3)_2$ (6.98 ± 2.08 kJ/mol) (Chai and Navrotsky 1996a,b) agrees with that estimated from the solvus of the $CaCO_3$-$FeCO_3$ system, 8.35 kJ/mol (Davies and Navrotsky 1983; Davidson et al. 1993). Increase in Fe content has opposite effects on stability of ordered and disordered phases. The ordered phase becomes more endothermic and hence less stable and the disordered ankerite becomes more exothermic and hence more stable with increasing Fe content (see Fig. 30). The enthalpy of formation of ordered dolomite $CaMg(CO_3)_2$ is –9.29 ± 1.97 kJ/mol. The enthalpy of disordering in dolomite (~ 25 kJ/mol) is larger than the disordering enthalpy in ankerite, $CaFe(CO_3)_2$ (~ 10 kJ/mol). These factors destabilize ordered $CaFe(CO_3)_2$ (Chai and Navrotsky 1996a,b).

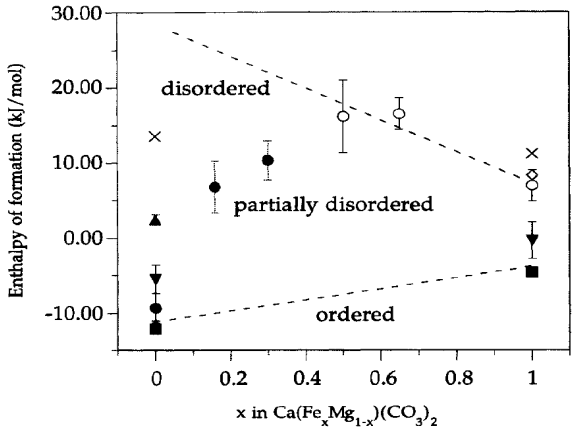

Figure 30. Enthalpy of formation of the ankerite solid solution. The circles are data from calorimetry, the squares are from lattice-energy calculations, the triangle is from (Navrotsky and Capobianco 1987), the inverted triangles are from (Holland and Powell 1990), and the diamond is calculated from the solvus. The Xs are for disordered phases calculated from solid-solution-mixing parameter (Davies and Navrotsky 1983). The Solid symbols indicate complete order; open symbols, complete disorder; and shaded symbols, partial disorder. Reprinted with permission from Chai and Navrotsky (1996a).

CARBONATE BEARING MULTICOMPONENT PHASES

Thermodyanmics of hydrotalcite-type layered double hydroxides (LDH)

Hydrotalcite-like compounds generally known as layered double hydroxides (LDH) are derivatives of the mineral hydrotalcite ($Mg_6Al_2(OH)_{16}(CO_3)\cdot 4H_2O$). The structure is made up of positively charged mixed metal hydroxide layers and the interlayers of anions and water appear to influence the hydroxide layer stacking sequences (Bellotto et al. 1996; Cavani et al. 1991; Radha et al. 2005; Thomas et al. 2006). The composition is $[M(II)_{1-x}M''(III)_x(OH)_2]^{x+}(A^{n-})_{x/n}\cdot mH_2O$, where M(II) = Mg, Ca, Fe, Co, Ni, Cu, Zn; M″ (III) = Al, Cr, Fe, Co and anions (A^{n-}) = CO_3^{2-}, Cl^-, NO_3^-, SO_4^{2-} polyoxometallates, organic anions. The interlayer regions are labile and readily undergo intercalation/deintercalation reactions and ion exchange (Radha et al. 2005b, 2007). Hydrotalcite is white mineral containing Mg-Al cations with carbonate anions and often occurs with other minerals such as serpentine and calcite. The Ni bearing analogue, takovite $[Ni_6Al_2(OH)_{16}(CO_3)\cdot 4H_2O]$, is found in karstic bauxites, with minerals such as carrboydite $[(Ni_{10}Cu_4Al_9(SO_4)_4(CO_3)_2(OH)_{43}\cdot 7(H_2O)]$, gaspeite $[Ni_{0.6}Mg_{0.3}Fe^{2+}_{0.1}(CO_3)]$ and in weathered Ni-sulfide deposits (Bish 1980).

A summary of enthalpies of formation of LDH with different cations and anions, obtained from high temperature oxide melt solution calorimetry, is given in Table 7 (Allada and Navrotsky 2002; Allada et al. 2005a,b, 2006). The third law entropy based on low temperature adiabatic heat capacity measurements suggested that the entropy contribution ($T\Delta S$ term) in Mg-Al-CO_3 LDH is 2-3 kJ/mol at room temperature (Allada et al. 2005a) and is within the uncertainties of formation enthalpies. The formation energetics of LDH with respect to their single cation hydroxides and carbonates and water contents (see Table 7) show about 5 to 20 kJ/mol stabilization (Allada and Navrotsky 2002; Allada et al. 2005a,b, 2006; Mazeina et al. 2008).

In $Mg_{1-x}Al_x(OH)_2(CO_3)_{x/2}\cdot mH_2O$, the enthalpies of formation from oxide and carbonate components change only slightly with variation in Al content (z) (Allada et al. 2005a), suggesting that the Mg/Al ratios are controlled by the activities of cations in solution and the pH rather than by big thermodynamic changes in the solid phase. Kinetic factors also

Table 7. Summary of heat of formation data for $M_{1-x}Al_x(OH)_2(CO_3)_{x/2}\cdot mH_2O$. Reproduced with permission from Allada et al. (2006). Copyright © 2006 The Clay Minerals Society.

Sample	ΔH_{dsol} (kJ/mol)	$\Delta_f H_{ox}$ (kJ/mol)	ΔH°_f (kJ/mol)	$\Delta_f H^{scc}$ (kJ/mol)
$Co_{0.68}Al_{0.32}(OH)_2(CO_3)_{0.16}$ $0.78H_2O$	226.98 ± 1.24 (4)	−42.80 ± 1.50	−1044.17 ± 2.54	−5.05 ± 2.86
$Co_{0.69}Al_{0.31}(OH)_2(CO_3)_{0.16}$ $0.68H_2O$	218.17 ± 1.28 (7)	−41.84 ± 1.32	−1006.26 ± 1.62	−4.42 ± 2.15
$Co_{0.70}Al_{0.30}(OH)_2(CO_3)_{0.16}$ $0.23H_2O$	212.18 ± 1.08 (6)	−49.22 ± 1.01	−877.34 ± 1.35	−11.04 ± 1.92
$Co_{0.76}Al_{0.24}(OH)_2(CO_3)_{0.12}$ $0.81H_2O$	228.50 ± 1.25 (4)	−43.51 ± 1.42	−991.79 ± 1.72	−9.78 ± 2.07
$Co_{0.80}Al_{0.20}(OH)_2(CO_3)_{0.10}$ $0.76H_2O$	215.97 ± 2.46 (4)	−35.23 ± 1.71	−933.36 ± 2.17	−3.88 ± 2.17
$Co_{0.83}Al_{0.17}(OH)_2(CO_3)_{0.09}$ $0.29H_2O$	183.47 ± 1.51 (4)	−35.00 ± 1.67	−777.09 ± 1.97	−5.13 ± 2.64
$Mg_{0.67}Al_{0.33}(OH)_2(CO_3)_{0.16}$ $0.70H_2O$	222.67 ± 1.26 (5)	−58.61 ± 1.79	−1284.65 ± 1.75	−11.01 ± 1.56
$Mg_{0.66}Al_{0.34}(OH)_2(CO_3)_{0.17}$ $0.69H_2O$	224.98 ± 1.42 (5)	−57.99 ± 1.68	−1292.07 ± 1.63	−11.62 ± 1.42
$Mg_{0.69}Al_{0.31}(OH)_2(CO_3)_{0.15}$ $0.30H_2O$	200.69 ± 0.85 (5)	−62.68 ± 1.66	−1168.52 ± 1.81	−16.61 ± 1.08
$Mg_{0.74}Al_{0.26}(OH)_2(CO_3)_{0.13}$ $0.39H_2O$	197.50 ± 1.18 (5)	−55.43 ± 1.43	−1165.98 ± 2.06	−10.49 ± 1.37
$Mg_{0.73}Al_{0.27}(OH)_2(CO_3)_{0.16}$ $0.83H_2O$	226.11 ± 1.06 (4)	−54.42 ± 1.87	−1297.19 ± 1.97	−7.20 ± 1.27
$Ni_{0.69}Al_{0.31}(OH)_2(CO_3)_{0.16}$ $0.37H_2O$	211.10 ± 1.01 (4)	−40.71 ± 1.16	−918.42 ± 1.21	−15.83 ± 1.28
$Ni_{0.66}Al_{0.34}(OH)_2(CO_3)_{0.17}$ $0.42H_2O$	208.33 ± 0.65 (4)	−43.70 ± 0.86	−904.031 ± 0.93	−8.98 ± 1.28
$Ni_{0.77}Al_{0.23}(OH)_2(CO_3)_{0.12}$ $0.33H_2O$	202.84 ± 1.03 (5)	−34.27 ± 1.21	−838.18 ± 1.26	−11.99 ± 1.58
$Ni_{0.67}Al_{0.33}(OH)_2(CO_3)_{0.17}$ $0.41H_2O$	217.89 ± 1.95 (5)	−40.07 ± 2.03	−908.42 ± 2.06	−19.46 ± 2.22
$Ni_{0.64}Al_{0.36}(OH)_2(CO_3)_{0.18}$ $0.46H_2O$	220.33 ± 1.38 (7)	−33.09 ± 1.48	−942.41 ± 1.53	−17.72 ± 1.72
$Zn_{0.67}Al_{0.33}(OH)_2(CO_3)_{0.17}$ $0.30H_2O$	192.84 ± 0.68 (4)	−45.32 ± 0.91	−993.04 ± 0.96	−21.97 ± 1.5

probably play a role. Thus one observes hydrotalcites with different compositions in a variety of conditions (Reichle 1986; Thevenot et al. 1989). However, the nature of divalent cations appears to have greater influence (5 to 20 kJ/mol) on thermodynamic stability (Allada et al. 2005a,b, 2006). The most stable phase is Zn-LDH, followed by the Ni-, Mg- and Co-LDH. These stability trends could not be rationalized based on any specific crystal chemical factors such as cation radius or M-O bond distortions. The solubility products for Co-Al, Mg-Al, Ni-Al and Zn-Al LDHs calculated from MINTEQ code (see Table 8) suggested a decrease in solubility compared to the mechanical mixture and agree with reported log K_{sp} values based on solubility measurements (Allada et al. 2006; Johnson and Glasser 2003).

Table 8. Solubility products for $M_{1-x}Al_x(OH)_2(CO_3)_{x/2}\cdot mH_2O$. Reproduced with permission from Allada et al. (2006). Copyright © 2006 The Clay Minerals Society.

Sample	log K_{sp}
$Ni_{0.69}Al_{0.31}(OH)_2(CO_3)_{0.16}\cdot 0.37H_2O$	2.24
$Co_{0.76}Al_{0.24}(OH)_2(CO_3)_{0.12}\cdot 0.81H_2O$	7.12
$Zn_{0.67}Al_{0.33}(OH)_2(CO_3)_{0.17}\cdot 0.30H_2O$	3.73
$Mg_{0.74}Al_{0.26}(OH)_2(CO_3)_{0.13}\cdot 0.39H_2O$	9.82

Dawsonite type compounds $MAl(OH)_2CO_3$ (M = Na, K, NH_4)

Dawsonite ($NaAlCO_3(OH)_2$ is a naturally occurring mineral with orthorhombic (*Imma*) structure having distorted $AlO_2(OH)_4$ and $NaO_4(OH)_2$ octahedra, and CO_3 groups (Corazza et al. 1977). Potassium dawsonite ($KAl(OH)_2CO_3$) and ammonium dawsonite ($NH_4Al(OH)_2CO_3$) are the other two known dawsonite-type compounds. Dawsonite occurs in various sedimentary rocks associated with volcanics or CO_2-rich alkaline thermal solutions and as hydrothermal alteration products of igneous rocks (Jackson et al. 1972; Baker et al. 1995; Sirbescu and Nabelek 2003). Several geochemical modeling studies have predicted the formation of dawsonite during the long term mineral sequestration of CO_2 in sodium rich brines (Ferrante et al. 1976; Xu et al. 2005; Zerai et al. 2006; Benezeth et al. 2007). However, dawsonite rarely forms in nature or in laboratory experiments under the conditions used in these simulations (Kaszuba et al. 2003). The equilibrium based experimental and modeling studies with following reaction has revealed that these inconsistencies in dawsonite stability field mainly arise due to lack of consistent thermodynamic data on aluminum hydroxide polymorphs and aluminum complexes, which lead to the gross underestimation of dissolved aluminum.

$$NaAlCO_3(OH)_2 \text{ (dawsonite)} + H_2O = Al(OH)_3 + Na^+ + HCO_3^-$$

The interactions among aluminum hydroxide/oxyhydroxide minerals and aqueous complexes compete with dawsonite to constrain aluminum solubility and thus influence the dawsonite stability field (Kaszuba et al. 2011).

Thermodynamic properties of dawsonite have been determined by copper block drop calorimetry and low temperature heat capacity (6 to 307 K) adiabatic calorimetry (Ferrante et al. 1976; Benezeth et al. 2007). These measurements showed $\Delta G^\circ_{f,\ 298.1K} = -1786 \pm 4$ kJ/mol, $\Delta H^\circ_{f,\ 298.1K} = -1964 \pm 4$ kJ/mol, $S^\circ_{298.1K} = 132 \pm 2$ J /K mol and $C^\circ_{p,\ 298.1K} = 142.6 \pm 0.4$ J/ K mol. The data for dawsonite dissolution has been calculated from the solubility measurements for the following dissolution reaction with under- and oversaturated solutions at 50-200 °C in basic media at 1.0 mol/kg NaCl.

$$NaAlCO_3(OH)_2\ (xl) + 2\ H_2O = Al(OH)_4^- + Na^+ + HCO_3^- + H^+$$

The thermodynamic parameters for the above reaction at 25 °C were calculated as $\Delta G° = 102.1$ kJ/mol, $\Delta H° = 97.0$ kJ/mol and $\Delta S° = -17.1$ J mol^{-1} K^{-1}.

Figure 31 shows the phase equilibrium diagram of dawsonite with bayerite and other common sandstone aquifer minerals such as quartz and albite in varying total aluminum and carbon concentrations at 100 °C (Benezeth et al. 2007). Such phase equilibrium study would be useful to understand the relative stability of dawsonite with respect to other minerals in geological sequestration conditions. Dawsonite is quite stable at wide range of pH when log[C] > −2.6 in absence of silica, (Fig. 31a) and has a lower limit of stability relative to bayerite at a pH 4.8 in presence of aluminum (Fig. 31b). Albite-bearing rocks in contact with saline fluids at 100 °C (Fig. 31a) dissolve in acidic solution after CO_2 introduction. This buffered pH drives the equilibrium to the region where dawsonite dominates over either boehmite or bayerite (Benezeth et al. 2007). This suggest that formation of dawsonite could trap CO_2 at lower pH

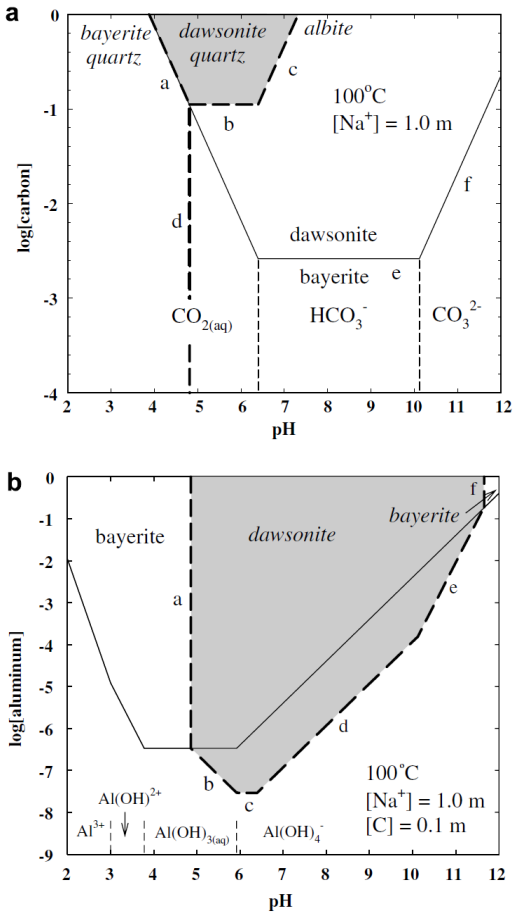

Figure 31. Stability diagram of dawsonite with respect to bayerite, albite and quartz. (a) log[C] versus pH and (b) log[Al] versus pH with [C] = 0.1 mol/kg in the presence of bayerite at an arbitrarily fixed [Na+]. Minerals in italics represent those present when silica is in the system. Reprinted with permission of Elsevier Science from Benezeth et al. (2007). Copyright © 2007 Elsevier Science.

limit due to buffering reaction of albite (Albite + HCO_3^- + H^+ = Dawsonite + 3 Quartz), when total dissolved carbon concentration is above 0.1 mol/ kg.

K_2CO_3-$CaCO_3$ double carbonates

The K_2CO_3-$CaCO_3$ binary system having three intermediate phases is generally found in wood ash, partly burned fir, hemlock, and other trees in the western United States and in the combustion of biomass fuels (Olanders and Steenari 1995). Butschliite and fairchildite are two polymorphs with composition $K_2Ca(CO_3)_2$. The third phase $K_2Ca_2(CO_3)_3$, is an incongruently melting phase (1083 K), which below 800 K decomposes to butschliite and $CaCO_3$. The structure of butschliite comprises atoms centered on mirror planes and the CO_3 groups situated on threefold axes, oriented normal to the *c* axis (Pabst 1974). In fairchildite and $K_2Ca_2(CO_3)_3$, a quarter of the cations are situated on the threefold axes and surrounded by CO_3 groups. The carbonate groups in Fairchildite forms a layered structure with half of the CO_3 groups orientationally disordered around a common C atom position (Pertlik 1981). The CO_3 groups are ordered but inclined relative to the (001) plane in $K_2Ca_2(CO_3)_3$.

The enthalpies of formation of double carbonates phases of K_2CO_3-$CaCO_3$ were determined by drop solution calorimetry in molten $2PbO{\cdot}B_2O_3$ at 974 K (Navrotsky et al. 1997). The enthalpies of formation from binary carbonates for butschliite and fairchildite polymorphs are −38.7 ± 3.2 kJ/mol and −5.1 ± 3.3 kJ/mol respectively and −7.2 ± 5.8 kJ/mol for $K_2Ca_2(CO_3)_3$. The entropy change for the formation of fairchildite is 40.9 ± 5.1 J/mol·K and of $K_2Ca_2(CO_3)_3$ is 39.4 ± 7.3 J/mol·K and it is zero for ordered butschliite. Thus butschliite is the stable low temperature polymorph and is calculated to transform to fairchildite at 822 K.

Rare earth oxycarbonates

The rare earth (Ln) metal oxides form oxycarbonate ($Ln_2O_2CO_3$) phases with CO_2 at low or moderate temperatures. They exist in three crystalline modifications known as I, IA and II. At ambient pressure, types I and IA are metastable compared with type II lanthanides lighter than Gd and Ln heavier than Gd, form only in type I structure (Turcotte et al. 1969). Thermodynamic data for the formation of rare earth oxy carbonates from their oxides (Ln_2O_3(xl) + CO_2(g) = $Ln_2O_2CO_3$(xl)) are given Table 9 and plotted against ionic potential in Figure 32 (Sjastad et al. 2012). The enthalpy, entropy, and free energy values derived from adiabatic shield calorimetry and drop solution calorimetry are found to be more accurate and are recommended over the data extracted from gas equilibration experiments or DTA studies.

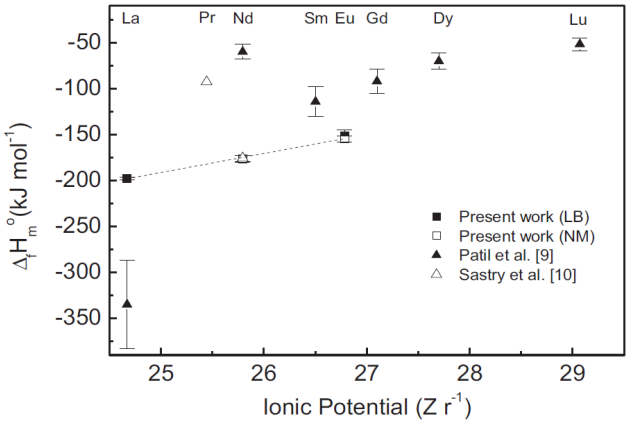

Figure 32. The enthalpy of formation of $Ln_2O_2CO_3$ from their oxide components at 298 K versus ionic potential. Reprinted with permission of Elsevier Science from Sjastad et al. (2012). Copyright © 2012 Elsevier Science.

Table 9. The standard enthalpies ($\Delta H_m°$) and entropies ($\Delta S_m°$) of formation for $Ln_2O_2CO_3$ from the component oxides Ln_2O_3 and CO_2. Modified from Sjastad et al. (2012) and reproduced with permission. Copyright © 2012 Elsevier Science.

Phase	$\Delta H_m°$ (*T*) (kJ/mol)	$\Delta S_m°$ (*T*) (J/ K·mol)	*T* (K)	Reference
		Calorimetric studies		
$La_2O_2CO_3$	−198.0 ± 1.7		298	Sjastad et al. (2012)
		−170.2 ± 0.6	300	Olafsen et al. (1999)
$Nd_2O_2CO_3$	−176.4± 4.7		298	Sjastad et al. (2012)
		−177.0 ± 0.6	300	Olafsen et al. (1999)
		−166.9 ± 0.9	900	Olafsen et al. (1999)
$Eu_2O_2CO_3$	−153.2 ± 7.2		298	Sjastad et al. (2012)
		DTA studies		
$La_2O_2CO_3$	−322 ± 48		1173	Patil et al. (1968)
$Pr_2O_2CO_3$	−88		813	Sastry et al. (1966)
$Nd_2O_2CO_3$	−50 ± 8		1063	Patil et al. (1968)
	−167		1003	Sastry et al. (1966)
$Sm_2O_2CO_3$	−105 ± 16		1023	Patil et al. (1968)
$Gd_2O_2CO_3$	−84 ± 13		973	Patil et al. (1968)
$Dy_2O_2CO_3$	−63 ± 9		933	Patil et al. (1968)
$Lu_2O_2CO_3$	−46 ± 7		863	Patil et al. (1968)
		Gas equilibration studies		
$La_2O_2CO_3$	−149	−126	1000-1300	Watanabe et al. (1986)
	−145.5 ± 5.0	−119.2 ± 5.0	773-1190	Shirsat et al. (2003)
$Nd_2O_2CO_3$	−213 ± 27	−195 ± 26	800–1100	Olafsen and Fjellvag (1999)
	−198.1 ± 5	−180 ± 5	775–1105	Shirsat et al. (2005)
$Sm_2O_2CO_3$	−131 ± 5	−127 ± 5	755–987	Shirsat et al. (2008)
$Eu_2O_2CO_3$	−155 ± 5	−153 ± 5	773–993	Shirsat et al. (2008)
$Gd_2O_2CO_3$	−187.9 ± 5	−197 ± 5	774–952	Shirsat et al. (2005)

Thermodynamics of calcium silicate carbonate minerals

The silicate carbonate minerals are another class of rock forming minerals that play an important role in CO_2-H_2O-rock interactions (Xu et al. 2004; Matter and Kelemen 2009). There are several silicate carbonates with well-refined crystal structures. The five common silicate carbonate minerals in the CaO-SiO_2-CO_2-H_2O system are spurrite, $Ca_5(SiO_4)_2(CO_3)$ (Smith 1960; Grice 2005), tilleyite, $Ca_5(Si_2O_7)(CO_3)_2$ (Louisnathan and Smith 1970; Grice 2005), scawtite, $Ca_7(Si_6O_{18})(CO_3)\cdot 2H_2O$ (Grice 2005), fukalite, $Ca_4Si_2O_6(OH)_2(CO_3)$ (Henmi et al. 1977) and the recently discovered galuskinite, $Ca_7(SiO_4)_3(CO_3)$ (Lazic et al. 2011).

Spurrite, $Ca_5(SiO_4)_2(CO_3)$ is an orthosilicate having separate layers of silicate and carbonate groups due to their different Lewis-base strengths (Grice 2005). The structure of scawtite $Ca_7(Si_6O_{18})(CO_3)\cdot 2H_2O$, is composed of a $[CaO_{6\text{-}8}]$ polyhedral sheet linked by Si_6O_{18} rings and isolated CO_3 groups parallel to (101) (Grice 2005). The enthalpies of formation determined by high-temperature oxide melt solution calorimetry for scawtite, and spurrite, are given in Table 10 (Zhang et al. 2013). The enthalpy of formation from the oxides is −689.5 ± 14.3 kJ/mol for scawtite and −455.1 ± 9.7 kJ/mol for spurrite, and the enthalpy

Table 10. Enthalpies of drop solution in molten lead borate at 702 °C , as well as the enthalpies of formation, of spurrite, scawtite and constituent oxides. Reproduced with permission from Zhang et al. (2013). Copyright © 2013 Elsevier Science.

Material	ΔH_{ds} (kJ/mol)	$\Delta H^\circ_{f,ox}$ (kJ/mol)	$\Delta H^\circ_{f,el}$ (kJ/mol)
Scawtite	940.2 ± 0.7 (11) [a]	−689.5 ± 14.3	−11564.5 ± 16.8
Spurrite	457.0 ± 1.2 (8)	−455.1 ± 9.7	−5845.5 ± 10.9
$CaCO_3$	189.6 ± 1.1 [b]	−178.9 ± 1.6	−1207.5 ± 1.3 [f]
CaO	−21.4 ± 1.9		−635.1 ± 0.9 [f]
SiO_2	38.4 ± 0.8 [c]		−910.7 ± 1.0 [f]
CO_2	32.1 ± 0.1 [d]		−393.5 ± 0.1 [f]
H_2O	69.0 ± 0.1 [d]		−285.8 ± 0.1 [f]
$CaSiO_3$	105.4 ± 0.7 [e]		
Ca_2SiO_4	121.44 ± 0.99 (8)		

NOTES:
[a] Uncertainty is two standard deviations of mean; number in paratheses is the number of expriments.
[b] Navrotsky et al. (1994)
[c] Schoenitz et al. (2001)
[d] Calculated from the heat capacity reported by Robie and Hemingway (1995).
[e] Chai and Navrotsky (1993)
[f] Robie and Hemingway (1995)

of formation from the elements is −11564.5 ± 16.8 kJ/mol for scawtite and −5845.5 ± 10.9 kJ/mol for spurrite. The entropy of formation for scawtite was estimated using the enthalpy of formation data with the earlier reported phase equilibrium results. The stability fields of spurrite and scawtite with calcium carbonate at 25 °C and 80 °C are shown in Figure 33. These diagrams suggest that spurrite forms in strongly oversaturated calcium solutions at 25 °C in solutions with a low aqueous silica activity. Scawtite on the other hand could precipitate in a wide range of Ca^{2+}/ H^+ activity ratio and higher a_{H4SiO4} value as well as at saturation with quartz. Calcite is stable at relatively low Ca^{2+}/ H^+ activity but in a very wide range of H_4SiO_4 activity. If the reservoir rock is sandstone, calcium carbonate would be the dominant product at 25 °C. However, scawtite and spurrite can form if the activity of Ca^{2+} is much higher

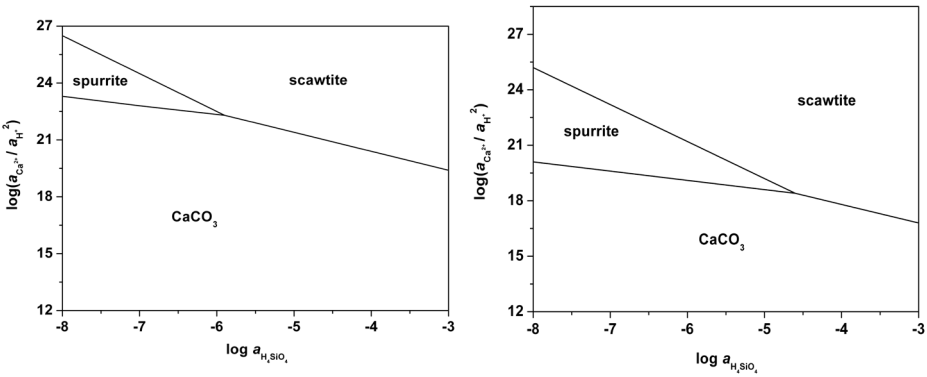

Figure 33. Mineral stability diagrams in the CaO-SiO_2-H_2O-CO_2 system at 25 and 80 °C. Reproduced with permission from Zhang et al. (2013). Copyright © 2013 Elsevier Science.

than that of H^+. Thus scawtite and spurrite may precipitate near the surfaces of dissolving silicate minerals, clays, or cement phases, as may occur in or near the caprocks in a CO_2 sequestration environment. At high temperatutre (80 °C) relevant to CO_2 sequestration, the expanded scawtite and spurrite stability fields suggest their favorable formation over calcite under moderate calcium concentration and pH by direct carbonation reactions.

A SUMMARY OF THERMODYNAMIC DATA FOR CARBONATE MINERALS

The thermodynamic data for different types of carbonate bearing minerals are summarized in Table 11 to give a bird's eye view of the data available in the literature.

CONCLUSIONS AND OUTLOOK

The thermodynamic properties of divalent binary carbonates MCO_3 and the ternary and higher order systems derived from them are dominated by three factors: the initial formation of amorphous phases, the competition between calcite, aragonite, vaterite, and dolomite structures in the crystalline state, and the mixing of cations. When the size mismatch of cations is small (e.g. Mg^{2+} and Fe^{2+}, Ca^{2+} and Sr^{2+}), disordered solid solutions occur, with positive heats of mixing and solvi reflecting lattice strain. When the size difference is larger, e.g. Mg^{2+} and Ca^{2+} or Mg^{2+} and Cd^{2+}, ordering of cations in alternate layers occurs, with negative heats of mixing and formation of ordered dolomite phases. There are also ternary carbonate phases in a number of other carbonate systems, as well as carbonate-containing layered double hydroxide phases and a number of carbonate silicate minerals. Though the thermodynamic picture of stability of these phases is improving, much work remains to be done. Because of the subtle effects of particle size, structural disorder, and inclusion/adsorption of water and organics, thermodynamic and structural and spectroscopic studies must go hand in hand. Kinetic and thermodynamic factors affecting carbonate reactions must be identified and separated. Interactions between carbonates and silicate minerals are important and need further study. To understand carbonate stability in aqueous and hydrothermal environments, the properties of the aqueous phase must be much better known, especially at high pressure, temperature, and salinity.

ACKNOWLEDGMENTS

This material is based upon work supported as part of the Center for Nanoscale Control of Geologic CO_2, an Energy Frontier Research Center funded by the U.S. Department of Energy, Office of Science, Office of Basic Energy Sciences under Award Number DE-AC02-05CH11231. We thank Tori Z. Forbes, Yin-Qing Zhang, Ozlem Sel, Di Wu, Olga Trofymulk, and Alexis Loulier for their contributions toward this project. We are especially thankful to Yin-Qing Zhang for putting together the thermodynamic data table of carbonate bearing minerals.

Table 11. Thermodynamic data of carbonate bearing minerals.

Name	Chemical Formula	ΔH_f from oxides kJ/mol	ΔH_f from elements kJ/mol	ΔG_f from elements kJ/mol	Reference
Natrite	Na_2CO_3	– 241.2 ± 0.8 [a]	– 1049.5 ± 0.4 [f]		Kiseleva et al. (1996), Robie et al. (1978)
Thermonatrite	$Na_2CO_3{\cdot}H_2O$	– 335.5 [f]	– 1429.7 [a]	–1286.1 [a]	Robie and Hemingway (1995)
Natron	$Na_2CO_3{\cdot}10\ H_2O$	– 412.76 [f]	–4079.39 [g]	–3427.66 [g]	Johnson et al. (1992)
Burkeite	$Na_6CO_3(SO_4)_2$			–3592.99 [g]	Johnson et al. (1992)
Cancrinite (NC2)	$Na_{7.770}[Al_{6.003}Si_{5.997}O_{24}](NO_3)_{1.474}(CO_3)_{0.146}{\cdot}2.175H_2O$	–871.65 ± 12.23 [a]	–14258.27 ± 17.34 [a]		Liu et al. (2007)
Cancrinite (NCS5)	$Na_{7.282}[Al_{5.854}Si_{6.146}O_{24}](NO_3)_{1.336}(CO_3)_{0.046}{\cdot}3.365H_2O$	–903.33 ± 15.72 [a]	–14258.27 ± 17.34 [a]		Liu et al. (2007)
Cancrinite (CAN7)	$Na_{7.571}[Al_{6.103}Si_{5.897}O_{24}](NO_3)_{1.242}(CO_3)_{0.113}{\cdot}3.533H_2O$	–871.65 ± 12.23 [a]	–14384.09 ± 15.76 [a]		Liu et al. (2007)
Cancrinite (CAN25)	$Na_{7.887}[Al_{5.982}Si_{6.018}O_{24}](NO_3)_{1.433}(CO_3)_{0.236}{\cdot}2.457H_2O$	–834.63 ± 9.08 [a]	–14207.51 ± 11.62 [a]		Liu et al. (2007)
Cancrinite (CAN50)	$Na_{7.725}[Al_{5.969}Si_{6.031}O_{24}](NO_3)_{1.234}(CO_3)_{0.261}{\cdot}2.829H_2O$	–844.94 ± 8.69 [a]	–14257.26 ± 11.32 [a]		Liu et al. (2007)
Cancrinite (CAN75)	$Na_{8.072}[Al_{6.055}Si_{5.945}O_{24}](NO_3)_{1.320}(CO_3)_{0.348}{\cdot}2.501H_2O$	–822.45 ± 9.75 [a]	–14292.44 ± 12.13 [a]		Liu et al. (2007)
Cancrinite (FB2-49)	$Na_{7.771}[Al_{5.956}Si_{6.004}O_{24}](CO_3)_{0.881}{\cdot}3.480H_2O$	–803.97 ± 12.08 [a]	–14524.07 ± 14.09 [a]		Liu et al. (2007)
Dawsonite	$NaAlCO_3(OH)_2$	–245.46 ± 3.00 [f]	–1963.97 ± 2.93 [b]	–1785.99 ± 2.95 [b]	Ferrante et al. (1976), Robie et al. (1978)
Sodalite	$Na_8Al_6Si_6O_{24}C_{l2}$	–899.9 ± 14.3 [a]	–11591.83 ± 16.0 [f]		Liu and Navrotsky (2007)
Magnesite	$MgCO_3$	–118.28 ± 1.37 [f]	–1113.28 ± 1.34 [f]	–1029.48 ± 1.38 [d]	Robie (1965), Robie et al. (1978)

Table 11. Continued.

Name	Chemical Formula	ΔH_f from oxides kJ/mol	ΔH_f from elements kJ/mol	ΔG_f from elements kJ/mol	Reference
Nesquehonite	$MgCO_3 \cdot 3H_2O$	–124.77 ± 0.43 [f]	–1977.26 ± 0.26 [b]	–1723.75 ± 0.50 [b]	Robie and Hemingway (1973), Robie et al. (1978)
Lansfordite	$MgCO_3 \cdot 5H_2O$			–2199.2	Woods and Garrels (1987)
Hydromagnesite	$Mg_5(CO_3)_4(OH)_2 \cdot 4H_2O$	–504.22 ± 1.88 [f]	–6514.86 ± 1.06 [b]	–5864.17 ± 1.09 [b]	Robie and Hemingway (1973), Robie et al. (1978)
Artinite	$Mg_2(OH)_2CO_3 \cdot 3H_2O$	–180.80 ± 0.94 [f]	–2920.61 ± 0.71 [b]	–2568.35 ± 0.75 [b]	Hemingway and Robie (1973), Robie et al. (1978)
Hydrotalcite	$Mg_{0.69}Al_{0.31}(OH)_2(CO_3)_{0.16} \cdot 0.30H_2O$	–62.91 ± 1.66 [a]	–1170.34 ± 1.81 [a]		Allada et al. (2005a,b)
Hydrotalcite	$Mg_{0.74}Al_{0.26}(OH)_2(CO_3)_{0.13} \cdot 0.39H_2O$	–55.44 ± 1.43 [a]	–1165.98 ± 2.06 [a]		Allada et al. (2005a,b)
Hydrotalcite	$Mg_{0.67}Al_{0.33}(OH)_2(CO_3)_{0.17} \cdot 0.69H_2O$	–58.61 ± 1.90 [a]	–1284.65 ± 1.97 [a]		Allada et al. (2005a,b)
Hydrotalcite	$Mg_{0.66}Al_{0.34}(OH)_2(CO_3)_{0.17} \cdot 0.70H_2O$	–57.99 ± 2.00 [a]	–1292.08 ± 2.05 [a]		Allada et al. (2005a,b)
Hydrotalcite	$Mg_{0.73}Al_{0.27}(CO_3)_{0.16}(OH)_{1.95} \cdot 0.83H_2O$	–55.99 ± 1.99 [f]	–1297.19 ± 1.97 [a]		Allada et al. (2005a,b)
Potassium carbonate	K_2CO_3	–234.4± 1.1 [a]	–991.1 ± 2.4 [f]		Kiseleva et al. (1996), Robie et al. (1978)
Butschliite	$K_2Ca(CO_3)_2$	–38.7 ± 3.2 [a]	–1824.0 ± 3.9 [f]		Robie et al. (1978), Navrotsky et al. (1997)
Fairchildite	$K_2Ca(CO_3)_2$	–5.1 ± 3.3 [a]	–1790.4 ± 4.0 [f]		Robie et al. (1978), Navrotsky et al. (1997)
	$K_2Ca_2(CO_3)_3$	–7.2 ± 5.8 [a]	–2821.1 ± 6.4 [f]		Robie et al. (1978), Navrotsky et al. (1997)
Aragonite	$CaCO_3$	–178.83 ± 1.68 [f]	–1207.43 ± 1.42 [a]	–1127.79 ± 1.46 [a]	Robie et al. (1978), Parker et al. (1971)
Calcite	$CaCO_3$	–178.77 ± 1.61 [f]	–1207.37 ± 1.34 [a]	–1128.84 ± 1.38 [a]	

Table 11. Continued.

Name	Chemical Formula	ΔH_f from oxides kJ/mol	ΔH_f from elements kJ/mol	ΔG_f from elements kJ/mol	Reference
Calcite	$CaCO_3$	–193.4 ± 0.7 [a]	–1221.99 ± 1.13 [f]		Kiseleva et al. (1996), Robie et al. (1978)
Vaterite	$CaCO_3$			–1125.540 ± 1.50 [b]	Turnbull (1973)
Monohydrocalcite	$CaCO_3 \cdot H_2O$	–183.86 ± 1.47 [f]	–1498.29 ± 1.17 [a,d]	–1361.600 ± 1.13 [a,d]	Hull and Turnbull (1973), Robie et al. (1978)
Ikaite	$CaCO_3 \cdot 6H_2O$	– 210.5 [f]	–2954.1 [a]	–2540.9 [a]	Robie and Hemingway (1995)
Dolomite	$CaMg(CO_3)_2$	–300.9 ± 0.5 [b]	–2324.5 ± 1.1 [b]	–2161.7 ± 1.1 [b]	Hemingway and Robie (1994)
Dolomite	$CaMg(CO_3)_2$			–2147.82 ± 2.20 [e]	Rock et al. (2001)
Huntite	$CaMg_3(CO_3)_4$	–516.00 ± 2.07 [f]	–4529.60 ± 1.57 [b]	–4203.42 ± 1.63 [b]	Robie et al. (1978), Hemingway and Robie (1973)
Meionite	$Ca_4Al_6Si_6O_{24}CO_3$	–522.8 [f]	–13881.4 [a]	–13131.8 [a]	Robie and Hemingway (1995)
Pirssonite	$Na_2Ca(CO_3)_2 \cdot 2H_2O$			–635.794 [g]	Johnson et al. (1992)
Gaylussite	$Na_2Ca(CO_3)_2 \cdot 5H_2O$			–3372.61 [g]	Johnson et al. (1992)
Rhodochrosite	$MnCO_3$	–110.52 ± 1.30 [f]	–889.27 ± 1.21 [d]	–816.05 ± 1.38 [d]	Robie, (1965), Robie et al. (1978)
Kutnahorite	$CaMn(CO_3)_2$			–1950.6	Woods and Garrels (1987)
Siderite	$FeCO_3$	–71.43 ± 3.08 [f]	–736.98 ± 2.26 [d]	–666.70 ± 2.09 [d]	Robie et al. (1978)
Siderite	$FeCO_3$	–84.95 ± 2.24 [f]	–750.5 ± 0.8 [a]		Chai and Navrotsky (1994), Robie et al. (1978)
Ankerite	$Ca(Fe_{0.1583}Mg_{0.8417})(CO_3)_2$	6.80 ± 3.45 [a]	–1964.65 ± 3.59 [f]		Chai and Navrotsky (1996 a,b), Robie et al. (1978)
Ankerite	$Ca(Fe_{0.2990}Mg_{0.7010})(CO_3)_2$	10.36 ± 2.64 [a]	–1914.73 ± 2.87 [f]		Chai and Navrotsky (1996 a,b), Robie et al. (1978)

Table 11. Continued.

Name	Chemical Formula	ΔH_f from oxides kJ/mol	ΔH_f from elements kJ/mol	ΔG_f from elements kJ/mol	Reference
Ankerite	$Ca(Fe_{0.4996}Mg_{0.5004})(CO_3)_2$	16.21 ± 4.80 [a]	–1842.80 ± 5.00 [f]		Chai and Navrotsky (1996 a,b), Robie et al. (1978)
Ankerite	$Ca(Fe_{0.6482}Mg_{0.3518})(CO_3)_2$	16.54 ± 2.10 [a]	–1793.51 ± 2.66 [f]		Chai and Navrotsky (1996 a,b), Robie et al. (1978)
Ankerite	$CaFe(CO_3)_2$	6.98 ± 2.08 [a]	–1687.17 ± 3.09 [f]		Chai and Navrotsky (1996 a,b), Robie et al. (1978)
Sphaerocobaltite	$CoCO_3$	–114.36 ± 1.10 [a]	–745.82 ± 1.68 [a]		Allada and Navrotsky (2002)
Co-Al hydrotalcite	$Co_{0.68}Al_{0.32}(OH)_2(CO_3)_{0.16}\cdot 0.779H_2O$	–42.80 ± 1.50 [a]	–1044.17 ± 2.54 [a]		Allada and Navrotsky (2002)
Co-Al hydrotalcite	$Co_{0.756}Al_{0.244}(OH)_2(CO_3)_{0.122}\cdot 0.805H_2O$	–43.51 ± 1.42 [a]	–991.79 ± 1.72 [a]		Allada and Navrotsky (2002)
Co-Al hydrotalcite	$Co_{0.756}Al_{0.244}(OH)_2(CO_3)_{0.1202}(NO_3)_{0.0018}\cdot 0.810H_2O$	–21.87 ± 3.47 [f]	–967.89 ± 3.33 [a]		Allada and Navrotsky (2002)
Malachite	$Cu_2CO_3(OH)_2$	–59.97 ± 3.29 [f]	–1053.95 ± 2.09		Richardson and Brown (1974), Robie et al. (1978)
Azurite	$Cu_3(OH)_2(CO_3)_2$	–87.37 ± 4.27 [f]	–1632.18 ± 2.00 [a]		Wagman et al. (1969), Robie et al. (1978)
Smithsonite	$ZnCO_3$	–68.81 ± 2.95 [f]	–812.78 ± 2.93 [a]	–731.48 ± 2.97 [a]	Parker et al. (1971), Robie et al. (1978)
Strontianite	$SrCO_3$	–234.88 ± 1.26 [b]	–1233.43 ± 2.09 [b]	–1153.04 ± 2.09 [b]	Adami and Conway (1966)
Strontianite	$SrCO_3$	–247.4 ± 3.3 [f]	–1231.4 ± 3.2 [a]		Kiseleva et al. (1994), Robie et al. (1978)
Otavite	$CdCO_3$	–98.90 ± 2.65 [f]	–750.61 ± 2.51 [a]	–669.44 ± 2.64 [a]	Wagman et al. (1968), Robie et al. (1978)
Witherite	$BaCO_3$	–269.63 ± 1.26 [b]	–1245.57± 3.35 [b]	–1165.61 ± 3.35 [b]	Adami and Conway (1966)

Table 11. Continued.

Name	Chemical Formula	ΔH_f from oxides kJ/mol	ΔH_f from elements kJ/mol	ΔG_f from elements kJ/mol	Reference
Witherite	$BaCO_3$	–268.29 ± 6.17 [f]	–1209.9 ± 5.8 [a]		Kiseleva et al. (1994), Robie et al. (1978)
Cerussite	$PbCO_3$	–90.43 ± 1.26 [b]	–703.38 ± 1.26 [b]	–629.69 ± 1.26 [b]	Adami and Conway (1966)
Rutherfordine	$(UO_2)(CO_3)$	–99.1 ± 4.2 [a]	–1716.4 ± 4.2 [a]	–1564.7 ± 1.8 [a]	Kubatko et al. (2005)
Andersonite	$Na_2Ca(UO_2)(CO_3)_3(H_2O)_5$	–710.6 ± 9.1 [a]	–5593.6 ± 9.1 [a]	–5651 ± 24 [a]	Kubatko et al. (2005)
Grimselite	$K_3Na(UO_2)(CO_3)_3(H_2O)$	–989.3 ± 14.0 [a]	–4431.6 ± 15.3 [a]	–4051.3 ± 1.8 [a]	Kubatko et al. (2005)
Barentsite	$Na_7AlH_2(CO_3)_4F_4$	N/A			
Shortite	$Na_2Ca_2(CO_3)_3$	N/A			
Zemkorite	$(Na,K)_2Ca(CO_3)_2$	N/A			
Tunisite	$NaCa_2Al_4(CO_3)_4(OH)_8Cl$	N/A			
Carletonite	$Na_4KCa_4Si_8O_{18}(CO_3)_4F{\cdot}H_2O$	N/A			
Spurrite	$Ca_5(SiO_4)_2(CO_3)$	N/A			
Tilleyite	$Ca_5Si_2O_7(CO_3)_2$	N/A			
Scawtite	$Ca_7Si_6O_{18}(CO_3){\cdot}2H_2O$	N/A			
Gaspeite	$(Ni,Mg,Fe)CO_3$	N/A			
Hydrozincite	$Zn_5(CO_3)_2(OH)_6$	N/A			
Minrecordite	$CaZn(CO_3)_2$	N/A			
Rosasite	$(Cu,Zn)_2CO_3(OH)_2$	N/A			
Aurichalcite	$(Cu,Zn)_5(CO_3)_2(OH)_6$	N/A			
Barytocite	$BaCa(CO_3)_2$	N/A			
Kampfite	$Ba_6(Si,Al)_8O_{16}(CO_3)_2Cl_2{\cdot}H_2O$	N/A			

Table 11. Continued.

Name	Chemical Formula	ΔH_f from oxides kJ/mol	ΔH_f from elements kJ/mol	ΔG_f from elements kJ/mol	Reference
Fencooperite	$Ba_6Fe_3Si_8O_{23}(CO_3)_2Cl_3 \cdot H_2O$	N/A			
Bussenite	$Na_2Ba_2FeTiSi_2O_7(CO_3)(OH)_3F$	N/A			
Tundrite	$Na_2Ce_2TiO_2(SiO_4)(CO_3)_2$	N/A			
Hydrocerussite	$Pb_3(CO_3)_2(OH)_2$	N/A			
Phosgenite	$Pb_2(CO_3)Cl_2$	N/A			
Ashburtonite	$Cu_4Pb_4Si_4O_{12}(HCO_3)_4(OH)_4Cl$	N/A			
Zellerite	$Ca(UO_2)(CO_3)_2 \cdot 5H_2O$	N/A			
Limoriite	$Y_2(SiO_4)(CO_3)$	N/A			
Kainosite	$Ca_2Y_2Si_4O_{12}(CO_3) \cdot H_2O$	N/A			
Caysichite	$Ca_4Y_4Si_8O_{20}(CO_3)_6(OH) \cdot 7H_2O$	N/A			
Ashcroftine	$K_5Na_5Y_{12}Si_{28}O_{70}(CO_3)_8(OH)_2 \cdot 8H_2O$	N/A			

Superscripts indicate the method: a. Solution calorimetry; b. Acid calorimetry; c. Oxide melt; d. Solubility equilibrium; e. Electrochemical cells; f. Calculated from ΔH_f from oxides or ΔH_f from elements; g. Calculated from computer models N/A = not available

REFERENCES

Adami LH, Conway KC (1966) Heats and free energies of formation of anhydrous carbonates of barium, strontium, and lead. US Bur Mines Rep Invest No. 6822, p 7

Addadi L, Raz S, Weiner S (2003) Taking advantage of disorder: Amorphous calcium carbonate and its roles in biomineralization. Adv Mater 15:959-970

Aizenberg J, Lambert G, Weiner S, Addadi L (2002) Factors involved in the formation of amorphous and crystalline calcium carbonate: A study of an ascidian skeleton. J Am Chem Soc 124:32-39

Allada RK, Navrotsky A (2002) Thermochemistry and aqueous solubilities of hydrotalcite-like solids. Science 296:721-723

Allada RK, Navrotsky A, Boerio-Goates J (2005a) Thermochemistry of hydrotalcite-like phases in the MgO-Al_2O_3-CO_2-H_2O system: A determination of enthalpy, entropy, and free energy. Am Mineral 90:329-335

Allada RK, Peltier E, Navrotsky A, Casey WH, Johnson CA, Berbeco HT, Sparks DL (2006) Calorimetric determination of the enthalpies of formation of hydrotalcite-like solids and their use in the geochemical modeling of metals in natural waters. Clays Clay Miner 54:409-417

Allada RK, Pless JD, Nenoff TM, Navrotsky A (2005b) Thermochemistry of hydrotalcite-like phases intercalated with CO_3^{2-}, NO_3^-, Cl^-, I^-, and ReO^{4-}. Chem Mater 17:2455-2459

Baker JC, Bai GP, Hamilton PJ, Golding SD, Keene JB (1995) Continental-scale magmatic carbon dioxide seepage recorded by dawsonite in the Bowen-Gunnedah-Sydney basin system, eastern Australia. J Sediment Res Sec A65:522-530

Bellotto M, Rebours B, Clause O, Lynch J, Bazin D, Elkaiem E (1996) A reexamination of hydrotalcite crystal chemistry. J Phys Chem 100:8527-8534

Benezeth P, Palmer DA, Anovitz LM, Horita J (2007) Dawsonite synthesis and reevaluation of its thermodynamic properties from solubility measurements: Implications for mineral trapping of CO_2. Geochim Cosmochim Acta 71:4438-4455

Beniash E, Aizenberg J, Addadi L, Weiner S (1997) Amorphous calcium carbonate transforms into calcite during sea urchin larval spicule growth. Proc R Soc London 264:461-465

Benson SM, Cole DR (2008) CO_2 sequestration in deep sedimentary formations. Elements 4:325-331

Bewernitz MA, Gebauer D, Long J, Colfen H, Gower LB (2012) A metastable liquid precursor phase of calcium carbonate and its interactions with polyaspartate. Faraday Discuss 159:291-312

Bischoff WD, Bishop FC, Mackenzie FT (1983) Biogenically produced magnesian calcite: inhomogeneities in chemical and physical properties; Comparison with synthetic phases. Am Mineral 68:1183-1188

Bish DL (1980) Anion-exchange in takovite: applications to other hydroxide minerals. Bull Mineral 103:170-175

Braybrook AL, Heywood BR, Jackson RA, Pitt K (2002) Parallel computational and experimental studies of the morphological modifications of calcium carbonate by cobalt. J Cryst Growth 243:336-344

Bruno M, Massaro RF, Prencipe M (2008) Theoretical structure and surface energy of the reconstructed {01.2} form of calcite ($CaCO_3$) crystal. Surf Sci 602:2774-2782

Burton BP (1987) Theoretical analysis of cation ordering in binary rhombohedral carbonate systems. Am Mineral 72:329-336

Busenberg E, Plummer LN (1989) Thermodynamics of magnesian calcite solid-solutions at 25 °C and 1 atm total pressure. Geochim Cosmochim Acta 53:1189-1208

Capobianco C, Navrotsky A (1987) Solid-solution thermodynamics in $CaCO_3$-$MnCO_3$. Am Mineral 72:312-318

Capobianco C, Burton BP, Davidson PM, Navrotsky A (1987) Structural and calorimetric studies of order-disorder in cadmium magnesium carbonate ($CdMg(CO_3)_2$). J Solid State Chem 71:214-223

Carlson WD (1983) Polymorphs of calcium carbonate and the aragonite-calcite transformation. Rev Mineral 11:191-225

Casey WH, Chai L, Navrotsky A, Rock PA (1996a) Thermochemistry of mixing strontianite [$SrCO_{3(s)}$] and aragonite [$CaCO_{3(s)}$] to form $Ca_xSr_{1-x}(CO_3)_{(s)}$ solid solutions. Geochim Cosmochim Acta 60:933-940

Casey WH, Rock PA, Chung J-B, Walling EM, McBeath MK (1996b) Gibbs energies of formation of metal-carbonate solid solutions. 2: the $Ca_xSr_{1-z}CO_{3(s)}$ system at 298 K and 1 bar. Am J Sci 296:1-22

Cavani F, Trifiro F, Vaccari A (1991) Hydrotalcite-type anionic clays: preparation, properties and applications. Catal Today 1:173-301

Chai L, Navrotsky A (1993) Thermochemistry of carbonatepyroxene equilibria. Contrib Mineral Petrol 114:139-147

Chai L, Navrotsky A (1994) Enthalpy of formation of siderite and its application in phase equilibrium calculation. Am Mineral 79:921-929

Chai L, Navrotsky A (1996a) Synthesis, characterization, and energetics of solid solution along the dolomite-ankerite join, and implications for the stability of ordered $CaFe(CO_3)_2$. Am Mineral 81:1141-1147

Chai L, Navrotsky A (1996b) Synthesis, characterization, and enthalpy of mixing of the $(Fe,Mg)CO_3$ solid solution. Geochim. Cosmochim. Acta 60:4377-4383

Chai L, Navrotsky A, Reeder RJ (1995) Energetics of calcium-rich dolomite. Geochim Cosmochim Acta 59:939-944

Christoffersen J, Rostrup E, Christoffersen MR (1991) Relation between interfacial surface tension of electrolyte crystals in aqueous suspension and their solubility; Asimple derivation based on surface nucleation. J Crystal Growth 113:599-605

Cohen LH, Klement W Jr (1973) Determination of high-temperature transition in calcite to 5 kbar by differential thermal analysis in hydrostatic apparatus. J Geol 81:724-726

Cole DR, Chialvo AA, Rother G, Vlcek L, Cummings PT (2010) Supercritical fluid behavior at nanoscale interfaces: Implications for CO_2 sequestration in geologic formations. Philos Mag 90:2339-2363

Colfen H, Antonietti M (2008) Mesocrystals and Non-classical Crystallization; John Wiley & Sons: Chichester, UK

Corazza E, Sabelli C, Vannucci S (1977) Dawsonite: new mineralogical data and structure refinement. Neues Jahrb Mineral Monatsh 381-397

Crawford WA, Fyfe WS (1964) Calcite-aragonite equilibrium at 100 °C. Science 144:1569-1570

Davidson PM (1994) Ternary iron, magnesium, calcium carbonates: a thermodynamic model for dolomite as an ordered derivative of calcite-structure solutions. Am Mineral 79:332-339

Davidson PM, Symmes GH, Cohen BA, Reeder RJ, Lindsley DH (1993) Synthesis of the new compound $CaFe(CO_3)_2$ and experimental constraints on the $(Ca,Fe)CO_3$ join. Geochim Cosmochim Acta 57:5105-5109

Davies PK, Navrotsky A (1983) Quantitative correlations of deviations from ideality in binary and pseudobinary solid solutions. J Solid State Chem 46:1-22

De CC, Peters T (1981) The solvus in the system manganese(II) carbonate-calcium carbonate. Contrib Mineral Petrol 76:394-400

de Leeuw NH, Parker SC (1998) Surface structure and morphology of calcium carbonate polymorphs calcite, aragonite, and vaterite: an atomistic approach. J Phys Chem B 102:2914-2922

De Yoreo JJ, Dove PM (2004) Materials science. Shaping crystals with biomolecules. Science 306:1301-1302

De Yoreo JJ, Vekilov PG (2003) Principles of crystal nucleation and growth. Rev Mineral Geochem 54:57-93

De Yoreo JJ, Wierzbicki A, Dove PM (2007) New insights into mechanisms of biomolecular control on growth of inorganic crystals. Cryst Eng Comm 9:1144-1152

De Yoreo JJ, Zepeda-Ruiz LA, Friddle RW, Qiu SR, Wasylenki LE, Chernov A.A, Gilmer GH, Dove PM (2009) Rethinking classical crystal growth models through molecular scale insights: Consequences of kink-limited kinetics. Cryst Growth Design 9:5135-5144

De Yoreo JJ, Waychunas GA, Jun Y-S, Fernandez-Martinez A (2013) *In situ* investigations of carbonate nucleation on mineral and organic surfaces. Rev Mineral Geochem 77:229-257

Demichelis R, Raiteri P, Gale JD, Quigley D, Gebauer D (2011) Stable prenucleation mineral clusters are liquid-like ionic polymers. Nat Commun 2:590

Doughty C (2010) Investigation of CO_2 plume behavior for a large-scale pilot test of geologic carbon storage in a saline formation. Transp Porous Media 82:49-76

Dousi E, Kallitsis J, Chrissanthopoulos A, Mangood AH, Dalas E (2003) Calcite overgrowth on carboxylated polymers. J Crystal Growth 253:496-503

Dove MT, Powell BM (1989) Neutron diffraction study of the tricritical orientational order/disorder phase transition in calcite at 1260 K. Phys Chem Miner 16:503-507

Duffy DM, Harding JH (2004) Growth of polar crystal surfaces on ionized organic substrates. Langmuir 20:7637-7642

Essene EJ (1983) Solid solutions and solvii among metamorphic carbonates, with applications to geologic thermobarometry. Rev Mineral Geochem 11:77-96

Faatz M, Gröhn F, Wegner G (2004) Amorphous calcium carbonate: Synthesis and potential intermediate in biomineralization. Adv Mater 16:996-1000

Falini G, Fermani S, Gazzano M, Ripamonti A (1998) Oriented crystallization of vaterite in collagenous matrixes. Chem Eur J 4:1048-1052

Ferrante MJ. Stuve JM, Richardson DW (1976) Thermodynamic Data for Synthetic Dawsonite. US Bur Mines p. 13

Ferrini V, De Vito C, Mignardi S (2009) Synthesis of nesquehonite by reaction of gaseous CO_2 with Mg chloride solution: Its potential role in the sequestration of carbon dioxide. J Hazardous Mater 168:832-837

Forbes TZ, Radha AV, Navrotsky A (2011) The energetics of nanophase calcite. Geochim Cosmochim Acta 75:7893-7905

Friedman GM (2005) Unusual occurrences: vaterite. An uncommon polymorph of $CaCO_3$. Carbonates Evaporites 20:181

Friedman GM Schultz DJ, Guo B, Sanders JE (1993) Vaterite (an uncommon polymorph of calcium carbonate): occurrences in boreholes demonstrate unexpected longevity. J Sediment Petrol 63:663-664

Garcia DJ, Shao H, Hu Y, Ray JR, Jun Y-S (2012) Supercritical CO_2-brine induced dissolution, swelling, and secondary mineral formation on phlogopite surfaces at 75-95 °C and 75 atm. Energy Environ Sci 5:5758-5767
Garrels RM, Thompson ME, Siever R (1960) Stability of some carbonates at 25 °C and one atmosphere total pressure. Am J Sci 258:402-418
Gebauer D, Coelfen H (2011) Prenucleation clusters and non-classical nucleation. Nano Today 6:564-584
Gebauer D, Voelkel A, Coelfen H (2008) Stable prenucleation calcium carbonate clusters. Science 322:1819-1822
Gilman JJ (1960) Direct measurements of the surface energies of crystals. J Appl Phys 31:2208-2218
Goldsmith JR (1967) Metastability and hangovers in crystals. Geochim Cosmochim Acta 31:913-919
Goldsmith, JR, Graf DL (1957) The system CaO-MnO-CO_2; Solid-solution and decomposition relations. Geochim Cosmochim Acta 11:310-334
Goldsmith JR, Graf DL (1958) Structural and compositional variations in some natural dolomites. J Geology 66:678-693
Goldsmith JR, Heard HC (1961) Subsolidus phase relations in the system $CaCO_3$-$MgCO_3$. J Geology 69:45-74
Gomez-Morales J, Hernandez-Hernandez A, Sazaki G, Garcia-Ruiz JM (2010) Nucleation and polymorphism of calcium carbonate by a vapor diffusion sitting drop crystallization technique. Crystal Growth Design 10:963-969
Gordon TM, Greenwood HJ (1970) The reaction dolomite + quartz + water = talc + calcite + carbon dioxide. Am J Sci 268:225-242
Goujon G, Mutaftschiev B (1976) On the crystallinity and the stoichiometry of the calcite surface. J Colloid Interface Sci 57:148-161
Gower LB (2008) Biomimetic model systems for investigating the amorphous precursor pathway and its role in biomineralization. Chem Rev 108:4551-4627
Graf DL, Goldsmith JR (1955) Dolomite-magnesian calcite relations at elevated temperatures and carbon dioxide pressures. Geochim Cosmochim Acta 7:109-128
Grice JD (2005) The structure of spurrite, tilleyite and scawtite, and relationships to other silicate-carbonate minerals. Can Mineral 43:1489-1500
Gupta YP, Santhanam AT (1969) Cleavage surface energy of calcite crystals. Acta Metall 17:419-424
Han YS, Hadiko G, Fuji M, Takahashi M (2006) Crystallization and transformation of vaterite at controlled pH. J Crys Growth 289:269-274
Hemingway BS, Robie RA (1973) Calorimetric determination of the standard enthalpies of formation of huntite, $CaMg_3(CO_3)_4$, and artinite, $Mg_2(OH)_2CO_3{\cdot}3H_2O$, and their standard Gibbs free energies of formation. J Res US Geol Surv 1:535-541
Hemingway BS, Robie RA (1994) Enthalpy and Gibbs energy of formation of dolomite, $CaMg(CO_3)_2$ at 298.15 K from HCl solution calorimetry. U.S. Department of the Interior, US Geol Surv Open-file Report 94-575
Henmi C, Kusachi I, Kawahara A, Henmi K (1977) Fukalite, a new calcium carbonate silicate hydrate mineral. Mineral J 8:374-381
Holland HD, Borcsik M, Munoz J, Oxburgh UM (1963) Coprecipitation of Sr^{2+} with aragonite and of Ca^{2+} with strontianite between 90 and 100 °C. Geochim Cosmochim Acta 27:957-977
Holland TJB, Powell R (1990) An enlarged and updated internally consistent thermodynamic dataset with uncertainties and correlations: The system K_2O-Na_2O-CaO-MgO-MnO-FeO-Fe_2O_3-Al_2O_3-TiO_2-SiO_2-C-H_2-O_2. J Metamorphic Geol 8:89-124
Hu Q, Zhang J, Becker U (2010) Growth process and crystallographic properties of ammonia-induced vaterite. Mater Res Soc Symp Proc p 1272, Paper: 1272-PP1203-1206
Hull H, Turnbull AG (1973) Thermochemical study of monohydrocalcite. Geochim Cosmochim Acta 37:685-694
Hwang S, Blanco M, Demiralp E, Cagin T, Goddard WA (2001) The MS-Q force field for clay minerals: application to oil production. J Phy Chem B 105:4122-4127
Irving AJ, Wyllie PJ (1973) Melting relations in calcium oxide-carbon dioxide and magnesium oxide-carbon dioxide to 36 kilobars with comments on carbon dioxide in the mantle. Earth Planet Sci Lett 20:220-225
Jackson JJr, Huggins CW, Ampian SG (1972) Synthesis and Characterization of Dawsonite. Bur Mines p. 19
Jacobs GK, Kerrick DM, Krupka KM (1981) The high-temperature heat capacity of natural calcite ($CaCO_3$). Phys Chem Miner 7:55-59
Jamieson JC (1953) Phase equilibrium in the system calcite-aragonite. J Chem Phys 21:1385-1390
Janczuk B, Chibowski E, Bialopiotrowicz T (1986) Time dependence wettability of quartz with water. Chem Pap 40:349-356
Johannes W, Puhan D (1971) Calcite-aragonite transition, reinvestigated. Contrib Mineral Petrol 31:28-38
Johnson CA, Glasser FP (2003) Hydrotalcite-like minerals ($M_2Al(OH)_6(CO_3)0.5{\cdot}xH_2O$, where M = Mg, Zn, Co, Ni) in the environment: Synthesis, characterization, and thermodynamic stability. [Erratum to document cited in CA138:388278]. Clays Clay Miner 51:357

Johnson JW, Oelkers EH, Helgeson HC (1992) SUPCRT92:A software package for calculating the standard molal thermodynamic properties of minerals, gases, aqueous species, and reactions from 1 to 5000 bar and 0 to 1000 °C. Computers Geosci 18:899-947

Kamhi SR (1963) On the structure of vaterite, $CaCO_3$. Acta Crystallogr 16:770-773

Kanakis J, Dalas E (2000) The crystallization of vaterite on fibrin. J Cryst Growth 219:277-282

Kanakis J, Malkaj P, Petroheilos J, Dalas E (2001) The crystallization of calcium carbonate on porcine and human cardiac valves and the antimineralization effect of sodium alginate. J Crystal Growth 223:557-564

Kaszuba JP, Janecky DR, Snow MG (2003) Carbon dioxide reaction processes in a model brine aquifer at 200 °C and 200 bars: implications for geologic sequestration of carbon. Appl Geochem 18:1065-1080

Kaszuba JP, Janecky DR, Snow MG (2005) Experimental evaluation of mixed fluid reactions between supercritical carbon dioxide and NaCl brine: Relevance to the integrity of a geologic carbon repository. Chem Geol 217:277-293

Kaszuba JP, Viswanathan HS, Carey JW (2011) Relative stability and significance of dawsonite and aluminum minerals in geologic carbon sequestration. Geophys Res Lett 38:L08404/08401-L08404/08405

Kerisit S, Parker SC, Harding JH (2003) Atomistic simulation of the dissociative adsorption of water on calcite surfaces. J Phy Chem B 107:7676-7682

Ketzer JM, Iglesias R, Einloft S, Dullius J, Ligabue R, de Lima V (2009) Water-rock-CO_2 interactions in saline aquifers aimed for carbon dioxide storage: Experimental and numerical modeling studies of the Rio Bonito Formation (Permian), southern Brazil. Appl Geochem 24:760-767

Kharaka YK, Campbell P, Thorden JJ, Thomas PB, Cole DR, Hovorka SD (2010) Geologic storage of carbon dioxide: Potential environmental impacts of CO_2-organic interactions. Geochim Cosmochim Acta 74:A511-A511

Kharaka YK, Cole DR, Thordsen JJ, Kakouros E, Nance HS (2006) Gas-water-rock interactions in sedimentary basins: CO_2 sequestration in the Frio Formation, Texas, USA. J Geochem Explor 89:183-186

Kiseleva IA, Kotelnikov AR, Martynov KV, Ogorodova LP, Kabalov JK (1994) Thermodynamic properties of strontianite-witherite solid solution $(Sr,Ba)CO_3$. Phys Chem Minerals 21:392-400

Kiseleva IA, Navrotsky A, Belitsky IA, Fursenko BA (1996) Thermochemistry of natural potassium sodium calcium leonhardite and its cation-exchanged forms. Am Mineral 81:668-675

Koenigsberger E, Gamsjager, H (1990) Solid-solute phase equilibria in aqueous solution. IV. Calculation of phase diagrams. Z Anorg Allg Chem 584:185-193

Koga N, Nakagoe Y, Tanaka H (1998) Crystallization of amorphous calcium carbonate. Thermochim Acta 318:239-244

Kubatko K-A, Helean KB, Navrotsky A, Burns PC (2005) Thermodynamics of uranyl minerals: Enthalpies of formation of rutherfordine, UO_2CO_3, andersonite, $Na_2CaUO_2(CO_3)_3(H_2O)_5$, and grimselite, $K_3NaUO_2(CO_3)_3H_2O$. Am Mineral 90:1284-1290

Kvamme B, Kuznetsova T, Uppstad D (2009) Modelling excess surface energy in dry and wetted calcite systems. J Math Chem 46:756-762

Lazic B, Armbruster T. Savelyeva VB, Zadov AE, Pertsev NN, Dzierzanowski P (2011) Galuskinite, $Ca_7(SiO_4)_3(CO_3)$, a new skarn mineral from the Birkhin gabbro massif, Eastern Siberia, Russia. Mineral Mag 75:2631-2648

Levchenko AA, Li G, Boerio-Goates J, Woodfield BF. Navrotsky A (2006) TiO_2 stability landscape: polymorphism,surface energy and bound water energetics. Chem Mater 18:6324-6332

Lee HS, Ha TH, Kim K (2005) Fabrication of unusually stable amorphous calcium carbonate in an ethanol medium. Mater Chem Phys 93:376-382

Lioliou MG, Paraskeva CA, Koutsoukos PG, Payatakes AC (2007) Heterogeneous nucleation and growth of calcium carbonate on calcite and quartz. J Colloid Interface Sci 308:421-428

Liu Q, Navrotsky A (2007) Synthesis of nitrate sodalite: An in situ scanning calorimetric study. Geochim Cosmochim Acta 71:2072-2078

Liu Q, Navrotsky A, Jove-Colon CF, Bonhomme F (2007) Energetics of cancrinite: Effect of salt inclusion. Microporous Mesoporous Mater 98:227-233

Louisnathan SJ, Smith JV (1970) Crystal structure of tilleyite. Refinement and coordination. Z Kristallog Kristallgeom Kristallphys Kristallchem 132:288-306

Lumsden DN, Chimahusky JS (1980) Relationship between dolomite nonstoichiometry and carbonate facies parameters. *In:* Concepts and Models of Dolomitization. Zenger DH, Dunham J, Ethington R (ed). Sot Econ Paleontol Mineral, p 123- 137

Mackenzie FT, Bischoff WD, Bishop FC, Loijens M, Schoonmaker J, Wollast R (1983) Magnesian calcites: low-temperature occurrence, solubility, and solid-solution behavior. Rev Mineral 11:87-144

Mann S, Heywood BR, Rajam S, Birchall JD (1988) Controlled crystallization of calcium carbonate under stearic acid monolayers. Nature 334:692-695

Manoli F, Dalas E (2002) The crystallization of calcium carbonate on sodium cholate. J Mater Sci Mater Med 13:69-73

Markgraf SA, Reeder RJ (1985) High-temperature structure refinements of calcite and magnesite. Am Mineral 70:590-600
Massaro FR, Pastero L, Rubbo M, Aquilano D (2008) Theoretical surface morphology of {0112} acute rhombohedron of calcite: A comparison with experiments and {1014} cleavage rhombohedron. J Cryst Growth 310:706-715
Matter JM, Kelemen PB (2009) Permanent storage of carbon dioxide in geological reservoirs by mineral carbonation. Nat Geosci 2:837-841
Mazeina L, Navrotsky A, Dyar D (2008) Enthalpy of formation of sulfate green rusts. Geochim Cosmochim Acta 72: 1143-1153
McHale JM, Auroux A, Perrotta AJ, Navrotsky A (1997) Surface energies and thermodynamic phase stability in nanocrystalline alumina. Science 277:788-791
Medeiros SK, Albuquerque EL, Maia FF, Caetano EWS, Freire VN (2007) First-principles calculations of structural, electronic, and optical absorption properties of $CaCO_3$ Vaterite. Chem Phys Lett 435:59-64
Meldrum FC, Colfen H (2008) Controlling mineral morphologies and structures in biological and synthetic systems. Chem Rev 108:4332-4432
Meldrum FC and Sear RP (2008) Now you see them. Science 322:1802-1803
Michel FM, MacDonald J, Feng J, Phillips BL, Ehm L, Tarabrella C, Parise JB, Reeder RJ (2008) Structural characteristics of synthetic amorphous calcium carbonate. Chem Mater 20:4720–4728
Morse JW, Casey WH (1988) Ostwald processes and mineral paragenesis in sediments. Am J Sci 288:537-560
Natoli A, Wiens M, Schroder H-C, Stifanic M, Batel R, Soldati AL, Jacob DE, Muller WEG (2010) Bio-vaterite formation by glycoproteins from freshwater pearls. Micron 41:359-366
Navrotsky A (2001) Thermochemistry of nanomaterials in nanoparticles and the environment. Rev Mineral Geochem 44:73-103
Navrotsky A (2004) Energetic clues to pathways to biomineralization: precursors, clusters, and nanoparticles. Proc Natl Acad Sci USA. 101:12096-12101
Navrotsky A (2009) Energetics of oxide nanoparticles. Int J Quantum Chem 109:2647-2657
Navrotsky A (2011) Nanoscale Effects on thermodynamics and phase equilibria in oxide systems. Chem Phys Chem 12:2207-2215
Navrotsky A, Capobianco C (1987) Enthalpies of formation of dolomite and of magnesian calcites. Am Mineral 72:782-787
Navrotsky A, Rapp R P, Smelik E, Burnley P, Circone S, Chai L, Bose K, Westrich HR (1994) The behavior of H_2O and CO_2 in high temperature lead borate solution calorimetry of volatile-bearing phases. Am. Mineral 79:1099-1109
Navrotsky A, Putnam RL, Winbo C, Rosen E (1997) Thermochemistry of double carbonates in the K_2CO_3-$CaCO_3$ system. Am Mineral 82:546-548
Navrotsky A, Mazeina L, Majzlan J (2008) Size-driven structural and thermodynamic complexity in iron oxides. Science 319:1635-1638
Navrotsky A, Ma C, Lilova K, Birkner N (2010) Nanophase transition metal oxides show large thermodynamically driven shifts in oxidation-reduction equilibria. Science 330:199-201
Okayama T, Keller DS, Luner P (1997) The wetting of calcite surfaces. J Adhes 63:231-252
Olafsen A, Fjellvag H (1999) Synthesis of rare earth oxide carbonates and thermal stability of $Nd_2O_2CO_3$ II. J Mater Chem 9:2697-2702
Olafsen A, Fjellvag H, Solen S, Atake T, Kawaji H, Matsuo K (1999) Heat capacities and entropies of $La_2O_2CO_3$ from T = (12 to 300) K and of $Nd_2O_2CO_3$ from T = (12 to 930) K, and their interpretation. J Chem Thermodyn 31:433-449
Olanders B, Steenari B-M (1995) Characterization of ashes from wood and straw. Biomass Bioenergy 8:105-115
Pabst A (1974) Synthesis, properties, and structure of $K_2Ca(CO_3)_2$, buetschliite. Am Mineral 59:353-358
Pach L, Hrabe Z, Komarneni S, Roy R (1990) Controlled crystallization of vaterite from viscous solutions of organic colloids. J Mater Res 5:2928-2932
Parker VB, Wagman DD, Evans WH (1971) Selected values of chemical thermodynamic properties. Tables for the alkaline earth elements (elements 92 through 97 in the standard order of arrangement). US Natl Bur Stand Tech Note p. 106
Patil KC, Chandrashekhar GV, George MV, Rao CNR (1968) Infrared spectra and thermal decompositions of metal acetates and dicarboxylates. Can J Chem 46:257-265
Pedersen TF, Price NB (1982) The geochemistry of manganese carbonate in Panama Basin sediments. Geochim Cosmochim Acta 46:59-68
Pertlik F (1981) Structural investigations of synthetic fairchildite, $K_2Ca(CO_3)_2$. Z Kristallogr 157:199-205
Pitcher MW, Ushakov SV, Navrotsky A, Woodfield BF, Li GS, Boerio-Goates J, Tissue BM (2005) Energy crossovers in nanocrystalline zirconia. J Am Ceram Soc 88:160-167
Plummer LN, Busenberg E (1982) The solubilities of calcite, aragonite, and vaterite in carbon dioxide-water solutions between 0 and 90 °C, and an evaluation of the aqueous model for the system calcium carbonate-carbon dioxide-water. Geochim Cosmochim Acta 46:1011-1040

Plummer LN, Busenberg E (1987) Thermodynamics of aragonite-strontianite solid solutions: Results from stoichiometric solubility at 25 and 76 °C. Geochim Cosmochim Acta 51:1393-1411

Plummer LN, Busenberg E, Glynn PD, Blum AE (1992) Dissolution of aragonite-strontianite solid solutions in nonstoichiometric $Sr(HCO_3)_2$-$Ca(HCO_3)_2$-CO_2-H_2O solutions. Geochim Cosmochim Acta 56:3045-3072

Pouget EM, Bomans PHH, Goos JACM, Frederik PM, de With G, Sommerdijk NAJM (2009) The initial stages of template-controlled $CaCO_3$ formation revealed by Cryo-TEM. Science 323:1455-1458

Pouget EM, Bomans PHH, Dey A, Frederik PM, de With G, Sommerdijk NAJM (2010) The development of morphology and structure in hexagonal vaterite. J Am Chem Soc 132:11560-11565

Quigley D, Rodger PM (2008) Free energy and structure of calcium carbonate nanoparticles during early stages of crystallization. J Chem Phys 128:221101-1–221101-4

Radha AV, Navrotsky A (2013) Manganese carbonate formation from amorphous and nanocrystalline precursors: Thermodynamics and geo-elctrochemical relevance. Am Mineral, submitted

Radha AV, Shivakumara C, Kamath PV (2005a) DIFFaX simulations of stacking faults in layered double hydroxides. Clays Clay Miner 53: 521-528

Radha AV, Kamath PV, Shivakumara C (2005b) Mechanism of the anion exchange reactions of the Layered Double Hydroxides (LDHs) of Ca and Mg with Al. Solid State Sciences 7:1180-1187

Radha AV, Kamath PV, Shivakumara C (2007) Conservation of order, disorder and 'crystallinity' during anion exchange reactions among the Layered Double Hydroxides (LDHs) of Zn with Al. J Phys Chem B 111:3411-3418

Radha, AV, Bomati-Miguel O, Ushakov SV, Navrotsky A, Tartaj P (2009) Surface enthalpy, enthalpy of water adsorption and phase stability in nanocrystalline monoclinic Zirconia. J Am Ceram Soc 92:133-140

Radha AV, Forbes TZ, Killian CE, Gilbert PUPA, Navrotsky A (2010) Transformation and crystallization energetics of synthetic and biogenic amorphous calcium carbonate. Proc Natl Acad Sci USA 107:16438-16443

Radha AV, Fernandez-Martinez A, Hu YD, Jun YS, Waychunas GA, Navrotsky A (2012) Energetic and structural studies of amorphous $Ca_{1-x}Mg_xCO_3{\cdot}nH_2O$ ($0 \le x \le 1$). Geochim Cosmochim Acta 90:83-95

Railsback LB (1999) Patterns in the compositions, properties, and geochemistry of carbonate minerals. Carbonates Evaporites 14:1-20

Raiteri P, Gale JD (2010) Water is the key to nonclassical nucleation of amorphous calcium carbonate. J Am Chem Soc. 132:17623-17634

Raiteri P, Gale JD, Quigley D, Rodger PM (2010) Derivation of an accurate force-field for simulating the growth of calcium carbonate from aqueous solution: A new model for the calcite-water interface. J Phys Chem C 114:5997-6010

Ranade MR, Navrotsky A, Zhang HZ, Banfield JF, Elder SH, Zaban A, Borse PH, Kulkarni SK, Doran GS, Whitfield H J (2002) Energetics of nanocrystalline TiO_2. Proc Natl Acad Sci 99:6476–6481

Redfern SAT, Salje E, Navrotsky A (1989) High-temperature enthalpy at the orientational order-disorder transition in calcite: Implications for the calcite/aragonite phase equilibrium. Contrib Mineral Petrol 101:479-484

Reeder RJ (1983) Crystal chemistry of the rhombohedral carbonates. Rev Mineral 11:1-47

Reeder RJ, Dollase WA (1989) Structural variation in the dolomite-ankerite solid-solution series: An x-ray, Moessbauer, and TEM study. Am Mineral 74:1159-1167

Reeder RJ, Markgraf SA (1986) High-temperature crystal chemistry of dolomite. Am Mineral 71:795-804

Reeder RJ, Sheppard CE (1984) Variation of lattice parameters in some sedimentary dolomites. Am Mineral 69:520-527

Reichle WT (1986) Synthesis of anionic clay minerals (mixed metal hydroxides, hydrotalcite). Solid State Ionics 22:135-141

Ren D, Gao Y, Fen Q (2013) Comparative study on nano-mechanics and thermodynamics of fish otoliths. Mater Sci Eng C 33:9-14

Ribbe PH, Rider RJ, Goldsmith JR (eds) (1987) Carbonates: Mineralogy and Chemistry. Reviews in Mineralogy, Volume 11. Mineralogical Society of America

Richardson DW, Brown RR (1974) Enthalpy of formation of malachite. Albany Metall Res Cent p. 5

Rieger J, Frechen T, Cox G, Heckmann W, Schmidt C, Thieme J (2007) Precursor structures in the crystallization/precipitation processes of $CaCO_3$ and control of particle formation by polyelectrolytes. Faraday Discussions 136:265-277

Roayne A, Bisschop J, Dysthe DK, (2011) Experimental investigation of surface energy and subcritical crack growth in calcite. J Geophys Res Solid Earth 116:B04204/04201-B04204/04210

Robie RA (1965) Heat and free energy of formation in herzenbergite, troilite, magnesite, and rhodochrosite calculated from equilibrium data. US Geol Surv Prof Pap. 525-D, 65-72

Robie RA, Hemingway BS (1973) Enthalpies of formation of nesquehonite, $MgCO_3{\cdot}3H_2O$, and hydromagnesite, $5MgO{\cdot}4CO_2{\cdot}5H_2O$. J Res US Geol Surv 1, 543-547

Robie RA, Hemingway BS, Fisher JR (1978) Thermodynamic properties of minerals and related substances at 298.15 K and 1 Bar (105 Pascals) pressure and at higher temperatures. US Geol Sur Bull 1452
Robie RA, Hemingway GS (1995) Thermodynamic properties of minerals and related substances at 298.15 K and 1 bar (105 Pascals) pressure and at higher temperatures. US Geol Sur Bull 2131
Rock PA, Mandell GK, Casey WH, Walling EM (2001) Gibbs energy of formation of dolomite from electrochemical cell measurements and theoretical calculations. Am J Sci 301:103-111
Rosenberg PE (1963) Synthetic solid solutions in the systems $MgCO_3$-$FeCO_3$ and $MnCO_3$-$FeCO_3$. Am Mineral 48:1396-1400
Sastry RLN, Yoganarasimhan SR, Mehrotra PN, Rao CNR (1966) Preparation, characterization, and thermal decomposition of praseodymium, terbium, and neodymium carbonates. J Inorg Nucl Chem 28:1165-1177
Schoenitz M, Navrotsky A, Ross N (2001) Enthalpy of formation of $CaSi_2O_5$, a quenched high-pressure phase with pentacoordinate silicon. Phys Chem Miner 28:57-60
Sel O, Radha AV, Dideriksen K, Navrotsky A (2012) Amorphous iron (II) carbonate: Crystallization energetics and comparison to other carbonate minerals related to CO_2 sequestration. Geochim Cosmochim Acta 87:61-68
Shao H, Ray JR, Jun Y-S (2010) Dissolution and precipitation of clay minerals under geologic CO_2 sequestration conditions: CO_2-brine-phlogopite interactions. Envir Sci Techn 44:5999-6005
Shirsat AN, Ali M, Kaimal KNG, Bharadwaj SR, Das D (2003) Thermochemistry of $La_2O_2CO_3$ decomposition. Thermochim Acta 399:167-170
Shirsat AN, Bharadwaj SR, Das D (2008) Thermochemistry of decomposition of $RE_2O_2CO_3$ (RE=Sm, Eu). Thermochim Acta 477:38-41
Shirsat AN, Kaimal KNG, Bharadwaj SR, Das D (2005) Thermochemical studies on $RE_2O_2CO_3$ (RE = Gd, Nd) decomposition. J Phys Chem Solids 66:1122-1127
Simmons G, Bell P (1963) Calcite-aragonite equilibrium. Science 139:1197-1198
Sirbescu M-LC, Nabelek PI (2003) Dawsonite: An inclusion mineral in quartz from the Tin Mountain pegmatite, Black Hills, South Dakota. Am Mineral 88:1055-1059
Sjastad AO, Fjellvag H, Helean KB, Navrotsky A (2012) Enthalpy of formation of $Ln_2O_2CO_3$ II (Ln = La, Nd, Eu) and thermodynamics of decomposition equilibria. Thermochim Acta 550:76-82
Smith JV (1960) Crystal structure of spurrite, $Ca_5(SiO_4)_2CO_3$. II. Description of structure. Acta Crystallogr 13:454-458
Sohnel O, Mullin JW (1982) Precipitation of calcium carbonate. J Cryst Growth 60:239-250
Speer AJ (1983) Crystal chemistry and phase relations of orthorhombic carbonates. Rev Mineral 11:145-190
Sperber CM, Wilkinson BH, Peacor DR (1984) Rock composition, dolomite stoichiometry, and rock/water reactions in dolomitic carbonate rocks. J Geol 92:609-622
Thevenot F, Szymanski R, Chaumette P (1989) Preparation and characterization of aluminum-rich zinc-aluminum hydrotalcite-like compounds. Clays Clay Miner 37:396-402
Thomas GS, Radha AV, Kamath PV and Kannan S (2006) Thermally induced polytype transformations among the Layered Double Hydroxides (LDHs) of Mg and Zn with Al. J Phys Chem B 110:12365-12371
Titloye JO, de Leeuw NH, Parker SC (1998) Atomistic simulation of the differences between calcite and dolomite surfaces. Geochim Cosmochim Acta 62:2637-2641
Tribello GA, Bruneval F, Liew CC, Parrinello M (2009) A Molecular Dynamics Study of the Early Stages of Calcium Carbonate Growth. J Phys Chem B 113:11680-11687
Turcotte RP, Sawyer JO, Eyring L (1969) Rare earth dioxymonocarbonates and their decomposition. Inorg Chem 8:238-246
Turnbull AG (1973) Thermochemical study of vaterite. Geochim Cosmochim Acta 37:1593-1601
Verch A, Antonietti M, Colfen H (2012) Mixed calcium-magnesium pre-nucleation clusters enrich calcium. Z Kristallogr Cryst Mater 227:718-722
Wade WH, Hackerman N (1959) Heats of immersion. II. Calcite and kaolinite, effect of pretreatment. J Phys Chem 63:1639-1641
Wagman DD, Evans WH, Parker VB, Halow I, Bailey SM, Schumm RH (1968) Selected values of chemical thermodynamic properties. Nat Bur Stand (US), Tech Notes No. 270-3, 264 pp
Wagman DD, Evans WH, Parker VB, Halow I, Bailey SM, Schumm RH (1969) Selected values of chemical thermodynamic properties. Nat Bur Stand p. 141
Walter LM, Morse JW (1984) Magnesian calcite stabilities: a reevaluation. Geochim Cosmochim Acta 48:1059-1069
Wang D, Wallace AF, De Yoreo JJ, Dove PM (2009) Carboxylated molecules regulate magnesium content of amorphous calcium carbonates during calcification. Proc Natl Acad Sci USA 106:21511-21516
Wang J, Becker U (2009) Structure and carbonate orientation of vaterite ($CaCO_3$). Am Mineral 94:380-386
Wang J, Becker U (2012) Energetics and kinetics of carbonate orientational ordering in vaterite calcium carbonate. Am Mineral 97:1427-1436
Watanabe Y, Miyazaki S, Maruyama T, Saito Y (1986) Dissociation pressure of lanthanum dioxide carbonate. J Mater Sci Lett 5:135-136

Wolf G, Gunther C (2001) Thermophysical investigations of the polymorphous phases of calcium carbonate. J Therm Anal Calorim 65:687-698

Wolf G, Konigsberger E, Schmidt HG, Konigsberger LC, Gamsjager H (2000) Thermodynamic aspects of the vaterite-calcite phase transition. J Therm Anal Calorim 60:463-472

Wolf G, Lerchner J, Schmidt H, Gamsjaeger H, Koenigsberger E, Schmidt P (1996) Thermodynamics of $CaCO_3$ phase transitions. J Therm Anal 46:353-359

Wolf SE, Muller L, Barrea R, Kampf CJ, Leiterer J, Panne U, Hoffmann T, Emmerling F, Tremel W (2011) Carbonate-coordinated metal complexes precede the formation of liquid amorphous mineral emulsions of divalent metal carbonates. Nanoscale 3:1158-1165

Woods TL, Garrels RM (1987). Thermodynamic Values at Low Temperature for Natural Inorganic Materials: An Uncritical Summary, Oxford University Press, New York, New York

Wyckoff RWG (1964) Crystal Structures. Volume 2: Inorganic Compounds RXn, $RnMX_2$, $RnMX_3$. Second Edition, Interscience Publishers

Xu T, Apps JA, Pruess K (2004) Numerical simulation of CO_2 disposal by mineral trapping in deep aquifers. Appl Geochem 19:917-936

Xu T, Apps JA, Pruess K (2005) Mineral sequestration of carbon dioxide in a sandstone-shale system. Chem Geol 217:295-318

Zerai B, Saylor BZ, Matisoff G (2006) Computer simulation of CO_2 trapped through mineral precipitation in the Rose Run Sandstone, Ohio. Appl Geochem 21:223-240

Zhang Y-Q, Radha AV, Navrotsky A (2013) Thermochemistry of two calcium silicate carbonate minerals: scawtite, $Ca_7(Si_6O_{18})(CO_3)\cdot 2H_2O$, and spurrite, $Ca_5(SiO_4)_2(CO_3)$. Geochim Cosmochim Acta 115:92-99

Zimmrmann HD (1971) Equilibrium conditions of the calcite/aragonite reaction between 150° and 350 °C. Nature 231:203-204